Mafalda Maria Robalo de Azevedo Aleixo Pereira
Licenciada em Bioquímica

Role of sympathetic innervation in obesity

Dissertação para obtenção do
Grau de Mestre em Bioquímica

Orientador: Ana I. Domingos, Investigadora Principal, Instituto Gulbenkian de Ciência
Co-orientador: Gonçalo J. L. Bernardes, Investigador Principal, Instituto de Medicina Molecular

FACULDADE DE CIÊNCIAS E TECNOLOGIA
UNIVERSIDADE NOVA DE LISBOA

Setembro, 2015

Mafalda Maria Robalo de Azevedo Aleixo Pereira
Licenciada em Bioquímica

Role of sympathetic innervation in obesity

Dissertação para obtenção do
Grau de Mestre em Bioquímica

Orientador: Ana I. Domingos, Investigadora Principal,
Instituto Gulbenkian de Ciência
Co-orientador: Gonçalo J. L. Bernardes, Investigador
Principal, Instituto de Medicina Molecular

Setembro, 2015

Role of sympathetic innervation in obesity

Acknowledgements

First of all, I would like to thank to Alekos Athanasiadis for introducing me to Ana Domingos. Then, obviously my acknowledgment goes to Ana Domingos for giving me the opportunity to develop my project in her lab and for teaching me that we are always able to do it on our own. I also thank to Gonçalo Bernardes for believing in this project and for being available every time I asked for help.

From the bottom of my heart, I thank to the "real" people in the lab: Elsa, Nadiya, Roksana, Andreia, Inês and Imogen. You were the ones that were really there, the ones that taught me everything and the ones that helped me every time I needed - sometimes I did not have to ask, you were already there. You girls rock!

Apart from the lab, other people were important during this 14 months journey: people from other labs that were always helpful, Krzysztof (who supported me during countless weekends), people from Unit of Citometry and Imaging (Gaby, Ânia, Pimpão, Cláudia 1, Cláudia 2 and Rui), animal house facility caretakers and technicians, histology technicians, canteen people (mainly Sofia that provided food at strange hours), maintenance team (especially João for being like a privative engineer), Pedro Cal from Gonçalo Bernardes' Lab and many other people that I am not being able to mention.

Funding agencies were fundamental to allow this work to be performed, namely Instituto Gulbenkian de Ciência, European Molecular Biology Organization and Fundação para a Ciência e Tecnologia.

I could not leave behind Professor Alice that since the beginning accepted to be my "connection" to the Faculty and was always (meaning even in the evening!) available to clarify my doubts and to give me support to keep going.

At last (but for sure no least!), my biggest thank goes to my family, to my boyfriend and to my friends. You all know that I would not survive to this without you!

"E compreendes que é desta fibra que são feitos os vencedores. Que é a persistência, a abnegação, o espírito de sacrifício e um certo *autismo* que separam os que conseguem dos que desistem."

Marta Elias, *in* Maria Capaz

List of publications

Part of the results presented in this thesis were published in the following reference (DOI 10.1016/j.cell.2015.08.055): Wenwen Zeng*, Roksana M. Pirzgalska*, **Mafalda M.A. Pereira**, Nadiya Kubasova, Andreia Barateiro, Elsa Seixas, Yi-Hsueh Lu, Albina Kozlova, Henning Voss, Gabriel G. Martins, Jeffrey M. Friedman and Ana I. Domingos. Sympathetic Neuro-adipose Connections Mediate Leptin-Driven Lipolysis. *Cell* **163**, 84-94 (2015).

The work was also presented through poster presentations at iMED Conference 6.0 (Lisbon, 2014), Sociedade Portuguesa de Bioquímica Meeting (Coimbra, 2014) and Sociedade Portuguesa de Neurociências Meeting (Póvoa de Varzim, 2015).

Abstract

Obesity is considered a world epidemic, but no efficient therapy is available so far. Besides, the anatomy of the adipose organ was not described in detail. Thus, different mechanisms were proposed to explain obesity condition. One of those is the MONA LISA hypothesis that states that Most Obesities kNown Are Low In Sympathetic Activity. However, this theory is based on measurements of norepinephrine decrease in the heart and there is no direct evidence of the role of sympathetic nervous system (SNS) in obesity.

In this work, PEGyDT-mediated sympathectomy was developed to specifically ablate the SNS, without affecting the central nervous system. This was achieved by PEGylation of diphtheria toxin, a strategy that is approved by Food and Drug Administration and used to modulate pharmacokinetics of several biopharmaceuticals clinically approved.

The results show that sympathectomy leads to irreversible obesity, without affecting food intake. SNS ablation also causes glucose tolerance and thermogenesis impairment. Moreover, it was discovered that the SNS is required for amphetamine effects and this is an additional mechanism of action for this anti-obesity drug, as it was thought that it had an exclusive effect in the brain to suppress appetite. Furthermore, the anatomy of adipose organ was revealed in detail using optical projection tomography coupled to tissue clearing. It was shown that not only the inguinal adipose organ contains nerve bundles and a network of vasculature, but also that in the proximity of these structures there is a lymph node. In the epididymal fat, granular substructures are present but not nerve bundles or lymph node.

In conclusion, a strategy to study the role of the SNS in obesity was developed and causality of MONA LISA hypothesis was demonstrated. Moreover, an additional mechanism of action for amphetamine was shown and neuroanatomy of adipose organs was described for the first time.

Keywords: Obesity, Sympathetic Nervous System, PEGylation, Amphetamine, Anatomy, Adipose organ

Resumo

A obesidade é considerada uma epidemia mundial, mas não se encontra disponível uma terapia eficiente. Além disso, a anatomia do orgão adiposo não foi descrita detalhadamente. Assim, diferentes mecanismos foram propostos para explicar a obesidade. Um deles é a hipótese da MONA LISA que defende que a maioria dos obesos apresentam baixa actividade simpática. Contudo, esta teoria baseia-se em medições da diminuição da norepinefrina no coração, não existindo evidência directa da função do sistema nervoso simpático (SNS) na obesidade.

Neste trabalho, a simpatectomização mediada pela PEGyDT foi desenvolvida para remover especificamente o SNS, não afectando o sistema nervoso central. Isto foi conseguido recorrendo à PEGilação da toxina da difteria, sendo esta uma estratégia aprovada pelo órgão que controla os alimentos e medicamentos e utilizada para modular a farmacocinética de vários fármacos aprovados clinicamente.

Os resultados mostram que a simpatectomização conduz a obesidade irreversível, sem afectar a ingestão de alimentos. A remoção do SNS altera a tolerância à glucose e a termogénese. Foi ainda descoberto que o SNS é necessário para os efeitos da anfetamina, sendo este um mecanismo adicional deste fármaco anti-obesidade uma vez que foi mostrado que este teria um efeito exclusivamente no cérebro, como supressor do apetite. A anatomia do órgão adiposo foi revelada detalhamente usando tomografia de projecção óptica associada à transparentização do tecido. Foi mostrado que o órgão adiposo inguinal não só contém nervos e uma rede de vasculatura, mas também que existe um nódulo linfático na proximidade destas estruturas. Na gordura epididimal, estão presentes sub-estruturas granulares, mas não existem nervos nem nódulos linfáticos.

Concluindo, foi desenvolvida uma estratégia para estudar a função do SNS na obesidade e foi desmonstrada a causalidade da hipótese da MONA LISA. Foi ainda mostrado um mecanismo de acção adicional para a anfetamina e a neuro-anatomia dos órgãos adiposos foi descrita.

Palavras-chave: Obesidade, Sistema Nervoso Simpático, PEGilação, Anfetamina, Anatomia, Órgão adiposo

Aims

The main aim of this work is to develop a tool that allows the ablation of sympathetic nervous system, without damaging the central nervous system.

After this is accomplished, the goal is to study the effects of sympathectomy on mice, in order to understand the role of sympathetic nervous system in obesity.

It is also intended to use amphetamine, with the purpose of studying the effects of an anti-obesity drug on mice lacking a functional sympathetic nervous system.

List of contents

List of Figures

List of abbreviations

3D Three-dimensional
5-HT 5-hidroxitriptamine
β_3-Tub β_3-Tubulin
ADHD Attention deficit hyperactivity disorder
ADP Adenosine diphosphate
AMPH Amphetamine
ANS Autonomic nervous system
BAT Brown adipose tissue
BBB Blood-brain barrier
BM Bone marrow
BMI Body mass index
BSA Bovine serum albumin
C Enzymatic or catalytic domain of diphtheria toxin
CNS Central nervous system
CT Computed tomography
Dapi 4',6-diamidino-2-phenylindole
DMEM Dulbecco's modified Eagle medium
DMSO Dimethyl sulfoxide
DNA Deoxyribonucleic acid
DT Diphtheria toxin
DTR Diphtheria toxin receptor
EF-2 Elongation factor 2
ELISA Enzyme-linked immunosorbent assay
EM Electron microscopy
ER Estrogen receptor
Fab Fragment antigen binding
FACS Fluorescence-activated cell sorting
FBS Fetal bovine serum
FDA Food and Drug Administration
Fen Fenfluramine
GTT Glucose tolerance test
HFD High fat diet
iDTR Cre-inducible diphtheria toxin receptor
IGC Instituto Gulbenkian de Ciência
IMDM Iscove's modified Dulbecco's medium
i.p. Intraperitoneal
mAb Monoclonal antibody
Mal α-maleimide

MALDI-TOF Matrix-assisted laser desorption / ionization – time of flight

M-CSF Macrophage colony stimulating factor

MIP Maximal intensity projection

MOG Myelin oligodendrocyte glycoprotein

MONA LISA Most Obesities kNown Are Low In Sympathetic Activity

MRI Magnetic resonance imaging

MS Mass spectrometry

MW Molecular weight

NAD Nicotinamide adenine dinucleotide

NCDs Non-communicable diseases

ND Normal diet

NE Norepinephrine

NHS N-hydroxysuccinimide

OPT Optical projection tomography

ORF Open reading frame

PBS Phosphate buffered saline

PEG Polyethylene glycol

PEGyDT PEGylated diphtheria toxin

Phen Phentermine

PNAC Protein & Nucleic Acid Chemistry

R Receptor-binding domain of diphtheria toxin

RT Room temperature

SCID Severe combined immunodeficiency

SDS-PAGE Sodium dodecyl sulfate polyacrylamide gel electrophoresis

SEM Standard error of the mean

SNS Sympathetic nervous system

Sulfo-SMCC Sulfosuccinimidyl 4-(N-maleimidomethyl)cyclohexane-1-carboxylate

T Transmembranar or translocation domain of diphtheria toxin

TH Tyrosine hydroxylase

TNF Tumor necrosis factor

UIC Unit of Imaging and Citometry

VMH Ventromedial hypothalamus

VTA Ventral tegmental area

1. Introduction

1.1. Obesity

Although only recognized by the American Medical Association in 2013 as a disease, obesity is now considered as the largest and fastest world global epidemic - the "globesity" [1,2]. It is a public health challenge that remains unsolved and consequences of this epidemic will lead to serious health disorders, if nothing is done immediately to overcome this problem [3,4].

Each year, overweight or obesity are the cause of 3 million deaths in the world [5]. In 2000, 300 million people worldwide were considered obese or overweight and, in 2008, the number was set at 2 billion [1,2,4]. Obesity is not restricted to developed countries, being estimated that 115 million people suffer from obesity-related problems in developing countries [1,2,4,6]. Furthermore, 10 % of children and adolescents are obese and this number is predicted to double in 2025 [1].

Overweight and obesity result in impaired quality of life as physical disabilities and psychological problems are caused by these conditions. Besides, they are also considered as risk factors for chronic diseases that are known as non-communicable diseases (NCDs), such as diabetes mellitus, cardiovascular diseases and cancer [1,2,6–8]. Overweight and obesity also lead to adverse metabolic effects on blood pressure, cholesterol, triglycerides and insulin resistance [4,5,9]. In addition, obesity causes premature mortality and large healthcare costs [1,2,7,8].

A simple definition for obesity is to consider it as excessive fat accumulation, leading to health risk [9]. This is achieved when consumed calories are higher than expended, resulting in energy imbalance [1,9]. More precisely, obesity is measured through body mass index (BMI), which is calculated dividing the weight (in kilograms) by the square of height (in meters) [1,9,10]. If BMI is 30 kg/m^2 or higher, the person is considered obese [1,10,11].

A body weight loss of 5 to 10 % improves insulin resistance and hypertension and this can be achieved with a lifestyle change (reduction in caloric intake and increase in physical activity) [2,8,12]. The problem is that compliance to adapt to a new lifestyle is very limited, so pharmacological approaches are seen as a tool to achieve weight loss [2,6,12]. As the awareness of healthier eating habits and exercise was not effective, drugs regimens are needed to achieve a meaningful and sustainable reduction in body weight [2].

1.2. Anti-obesity therapy

There are now three main approaches to cope with obesity that suffer from a number of limitations:

- Changes in lifestyle (diet and physical activity), which are not effective. Most patients regain weight shortly after therapy end and, in some, regain occurs even during therapy.
- Bariatric surgery (bypass or gastric banding), which is effective for weight loss because it reduces the size of the stomach, thus reducing food intake, but it has drawbacks such as surgical complications, need for reoperation and perioperative mortality. Moreover, it is a very expensive procedure.
- Pharmacotherapy, that is used to promote weight loss and also to increase patients' compliance to lifestyle changes and will be discussed in detail below [1,2,8,10,13].

Drugs are used to assist and maintain weight loss because a lifestyle modification is not effective. In 2009, 1.5 million obesity-related prescriptions were dispensed [10]. Weight loss pharmacotherapy is prescribed to those with a BMI of 30 kg/m^2 or above or to those with a BMI of 27 kg/m^2 or above with an obesity-related condition (for instance, high blood pressure and diabetes) [14].

An anti-obesity drug is considered efficient when it is effective for 10 % weight reduction and improves overweight-dependent conditions; it is safe for long-term use without losing efficiency; the side effects are tolerable or transitory; it is not addictive; and its mechanism of action is known [1,2,12,15,16]. None of the existing drugs fulfill the mentioned characteristics [8]. As a consequence, there is an urgent need for the development of more selective, safer and more efficient drugs for obesity treatment [12].

Until 1940, amphetamine (AMPH) was used as an anti-obesity drug, but after World War II, it became a drug of abuse, leading to the search for safer alternatives in the field of sympathomimetic drugs, which inhibit norepinephrine (NE) re-uptake [17,18]. Between 1973 and 1996, dexfenfluramine and ephedrine were developed. Despite causing primary pulmonary hypertension, dexfenfluramine was approved by Food and Drug Administration (FDA) but one

year later was withdrawn because of cardiac toxicity. Ephedrine was used for asthma treatment, but it was proven to increase thermogenesis and reduce appetite, so it was also used as an anti-obesity drug. In 1994, Jeffrey M. Friedman discovered leptin and it was demonstrated that the lack of this hormone leads to obesity and also that treatment with leptin reverses this situation. After this, more centrally acting drugs were developed but, so far, none of them proved to be efficient [17].

The classification of agents to treat obesity is done according to their mechanisms of action. Hence, these drugs can be divided in three groups: those that reduce food intake; those that alter metabolism and those that increase thermogenesis or energy expenditure [12,19]:

- Appetite suppressant

Food intake reduction is achieved either by causing a delay in the onset of a meal or by achieving earlier satiety. This group of drugs includes monoamines acting on noradrenergic, serotonin, dopamine, and histamine receptors. Some peptides and neuropeptides also inhibit the appetite such as leptin; neuropeptide-y receptor antagonists; cholecystokinin; ghrelin antagonist; and pancreatic hormones (glucagon and insulin) [19].

The activation of the α_1- and β_2-adrenoceptors decreases food intake. These receptors are activated if drugs that release NE or block NE re-uptake are used. The same effect in food intake is detected if 5-hidroxitriptamine (5-HT), most known as serotonin, receptors (5-HT1 and 5-HT2) are activated. This activation is achieved using drugs that block 5-HT re-uptake, such as fluoxetine, sertraline, and fenfluramine (Fen) or providing 5-HT to the receptors [17,19].

Sympathomimetic drugs approved by FDA include: benzphetamine, phentermine (Phen) and diethylpropion (release NE); mazindol and sibutramine (block NE re-uptake); and phenylpropanolamine (activates adrenoceptors) [13,17,19]. Sympathomimetic drugs that were not approved are in the market carrying a warning label (AMPH and methamphetamine) or were never on the market (fenproporex and chlobenzorex) [19].

- Alter metabolism (to induce catabolism and inhibit anabolism)

The strategies used so far were directed to pre and post-absorptive mechanisms in order to modify fat absorption or metabolism. Pre-absorptive mechanisms aim to influence digestion and absorption of macronutrients, while post-absorptive mechanisms aim to enhance lipolysis, inhibit lipogenesis and affect fat distribution between inguinal and visceral sites. Xenical (orlistat), that inhibits pancreatic lipase and reduces intestinal digestion of fat, is the only drug of this group approved by FDA [1,2,10,12–14,17,19].

- Increase thermogenesis

This type of drugs aims to mimic the physiologic effects of exercise, that increases energy expenditure [19]. Although this type of drugs were not approved for obesity treatment, ephedrine was approved to relax bronchial smooth muscle in asthma patients and caffeine inhibits adenosine receptors and phosphodiesterase. Both were proved to increase thermogenesis and were used as anti-obesity treatment [12,17,19].

1.2.1. Fen and AMPH

In the 70s and 80s, Fen (Figure 1.1 A) was widely used as an anti-obesity therapy. It is known to increase serotonin release and inhibit serotonin re-uptake, so it is considered as a nonselective serotonin agonist, acting on 5-HT2A, 5-HT2B, and 5-HT2C receptors [8,13,19]. A therapy using Fen together with the Phen adrenergic drug resulted in a more effective weight loss with fewer side effects when compared to single drug therapies. Despite approval of both drugs by FDA, the combined therapy was not approved but was widely used and became known as the Fen/Phen therapy. The unwanted side effects arose in the form of valvular heart disease and this led to the withdrawal of Fen and dexfenfluramine, in 1997 [1,19,20].

AMPH, the contracted form of α-methyl-β-phenethylamine (Figure 1.1 B), was primarily used in the treatment of attention deficit hyperactivity disorder (ADHD) and narcolepsy, and only later it was used as an anti-obesity drug. In the beginning, it was freely available without prescription but then it became a highly restricted controlled drug [17,19,21]. Amphetamines were first used to treat obesity in the 30s and after that many AMPH-like agents were approved [22]. Its mechanism of action consists in stimulating the release of NE and dopamine, acting on the satiety centers of the brain [6]. This is a possible mechanism because amphetamines are derivatives of phenylethylamine which is the backbone of monoamine neurotransmitters such

as dopamine, NE and epinephrine [6,17,19,21–23]. It is also established that NE is responsible for the appetite suppressant effect, while dopamine is responsible for the risk of habituation [17,19]. Apart from the therapeutic efficacy, AMPH has psychiatric-related adverse effects for the reason that this is a sympathomimetic drug, thus stimulating the central nervous system (CNS). Many cases of recreational abuse and addiction were reported, as well as cardiovascular effects such as, tachycardia and increased blood pressure [6,17,19,21–23]. In addition, the long term (one year or more) efficacy is not proven [22,24,25]. All these drawbacks limited the therapeutic use and, nowadays, amphetamines are not clinically approved as a weight loss therapy [6,22,23].

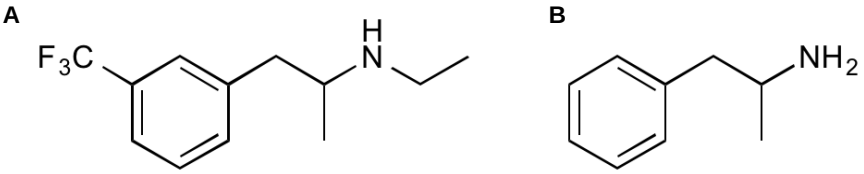

Figure 1.1 – Fen (A) and AMPH (B) chemical structures.

Many sympathomimetic drugs were clinically approved but were withdrawn from the market because of its undesirable side effects (the major concern is the cardiovascular toxicity). Therefore, many anti-obesity drugs are being developed and tested and their approval is being carefully done [1,19,23].

It has been suggested that some patients are insensitive to pharmacological agents, leading to the theory that there are several chemical mechanisms causing obesity [8]. In addition to the absence of efficient treatment, until the discovery of leptin hormone, the adipose tissue was considered only as an energy depot and was not accepted as an endocrine organ [26]. As an endocrine organ, adipose tissue is responsible for the synthesis and secretion of several hormones active in a variety of processes, such as control of nutritional intake, sensitivity to insulin, mediation of inflammatory processes or stimulation of signaling pathways [27,28]. The adipose organ is considered as an inguinal or a visceral organ, based on body location [28–30]. Although it is now considered as an organ, no anatomical characterization was made so far to describe the adipose tissue.

1.3. Fat characterization and Optical Projection Tomography (OPT)

The anatomy of adipose organ has been mostly studied with classical histology methods or electron microscopy (EM) [31]. These methods are suitable for histological analysis at a microscopic spatial scale, but do not give a three-dimensional (3D) perspective of the organization of the organ as a whole. The same applies to optical methods such as confocal or multiphoton microscopy [32,33]. At macroscopic spatial scale, methods such as magnetic resonance imaging (MRI) or computed tomography (CT) allow the measurement of whole body fat distribution [34–36]. However, all of these methods lack the spatial resolution that is required for visualizing structures within an organ. 3D description is important as the health of an organ can be accessed through visualization of its anatomical features.

OPT is a technique with physical principles similar to X-ray CT/gamma radiation, which uses a different wavelength (mainly, in the visible range) [37]. A full series of projections of the whole sample is acquired from multiple angles, typically 800 to 1600 angles, and from this series of projections a stack of axial slices is reconstructed through back-projection reconstruction. The slice reconstruction assumes perfect parallel projection, so scattering of light passing through tissues is minimized by clearing of the specimen [38]. Unlike most methods currently available, OPT coupled to tissue clearing is the only method suitable for imaging whole-mount samples with a spatial scale that lies in the order of centimeters.

The non-efficient anti-obesity therapy associated with lack of knowledge regarding adipose organ anatomy, led scientific community to search for different mechanisms to explain obesity condition. One hypothesis, released in 1991, states that Most Obesities kNow Are Low In Sympathetic Activity (MONA LISA), meaning that obesity is related to a decrease in sympathetic nervous system (SNS) activity [39].

1.4. MONA LISA hypothesis

In the process of trying to understand the control of body composition, many theories were developed. Some of them are listed below:

- Glucostatic hypothesis – states the role of blood glucose in the food intake. According to this hypothesis, an increase in blood glucose level leads to a reduction of food intake;
- Lipostatic hypothesis – says that food ingestion is decreased after leptin action on the hypothalamus;
- Gastrointestinal control of food intake hypothesis – defends that gastrointestinal hormones are able to lower food intake;
- Thermoregulatory hypothesis – states that the autonomic nervous system (ANS) is involved in the control of food intake through the production and loss of heat. This implies that body temperature and weight are strictly associated. According to this hypothesis, subjects with a higher body temperature and/or lower sympathetic activity eat a higher quantity of food to reverse this condition [40].

Apart from body composition control, the mechanisms specifically underlying obesity were also a focus of research. The systems involved on this control are: the endocrine system involving adrenal glucocorticosteroids, hyperphagia and SNS [39].

There were reasons to believe that the activation of the SNS would cause an increase in energy expenditure and a decrease in food intake. Therefore, the involvement of the ANS in the regulation of energy balance and body weight has been proposed [39]. In addition, it was proven that there are alterations of the SNS in the pathophysiological mechanisms of obesity. This is how MONA LISA hypothesis, an acronym for Most Obesities kNown Are Low In Sympathetic Activity, arose (Figure 1.2). This hypothesis states that obesity is related with an alteration in the sympathetic activity [39,41].

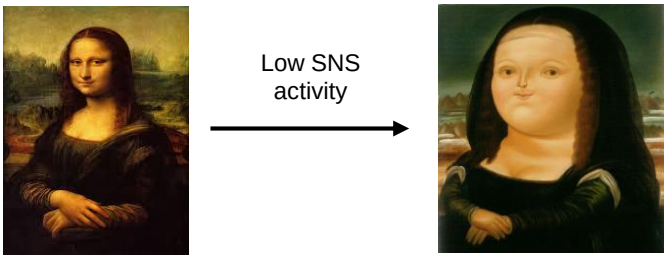

Figure 1.2 – Schematic representation of MONA LISA hypothesis [41].

Ultimately, it is the nutrient intake that influences the body weight stability and the regulatory processes, but food intake and energy expenditure are highly controlled. In addition, metabolic and neuroendocrine mechanisms also play a role in body weight maintenance. It is believed that to maintain energy balance there is a need to post-prandially (following food ingestion) activate the peripheral SNS. This activation depends on the integration of signals related to food intake in the brain. Interestingly, the level of sympathetic activation depends on diet composition, which becomes important in the pathogenesis of obesity and metabolic syndrome [40]. As consequence, a fasting state has implications in sympathetic activity, namely:

- The decrease of sympathetic activity could be a mechanism by which body conserves calories. Therefore, its increase could be a useful obesity treatment;
- The “fight or flight” survival response is compromised in subjects with a lower sympathetic activity [42].

The reduction of food intake by post-ingestional activation of sympathetic activity has been proved experimentally. In case of a lesion in the ventromedial hypothalamus (VMH), a reduction of sympathetic activity occurs. Consequently, a reduced sympathetic activity induces a decrease in energy expenditure that leads to a reduction of post-ingestional thermogenesis, which in turn contributes to obesity. In summary, both a reduction of satiety signals and a decrease in post-ingestional energy expenditure can explain an increase of body weight. Therefore, an increase in food intake associated to a reduced activity of the SNS could be the cause of obesity. Experiments that measured the sympathetic activity and food intake simultaneously were also performed to demonstrate the feedback between the SNS and food intake. It was shown that, before food intake ending, sympathetic activity rises, meaning that the sympathetic discharge is a satiety signal [39,40]. Experiments also proved that activity of the

rat SNS is reduced after two days of fasting and that this is reversed when the animals are in the re-fed period. On the other hand, increased sympathetic activity was reported in the heart of mice that were overfeed [39,42,43].

The measurement of the low-frequency of heart rate variability was presented as a non-invasive marker of sympathetic activity, but it was also reported as a poor marker because different situations, such as ischemia and exercise, modify the cardiac sympathetic drive [40,44]. Also, techniques using NE turnover were developed to measure the sympathetic activity. One of those techniques injects [^{3}H]-NE and the rate of disappearance is measured. Another method to assess NE turnover uses α-methylparatyrosine to inhibit tyrosine hydroxylase (TH), an enzyme involved in NE biosynthesis. After inhibition of NE biosynthesis, the rate of NE decrease is measured [42]. These techniques allow the *in vivo* quantification of sympathetic activity in an organ-specific manner [42,43]. A direct way to analyze the role of SNS activity in obesity would be to ablate it, but there is no way to do it without affecting the CNS as well.

1.5. Ablation of central and peripheral nervous systems

In order to study the function of a gene, not only the mouse genome should be altered by conventional transgenic and gene-targeted approaches, but also conditions such as timing, cell-type, and tissue specificity of genes should be controlled. The Cre/loxP system was generated to create tissue-specific knockout mice. Two different genetically engineered mouse lines are needed to have a tissue-specific gene deletion: Cre- and loxP-containing strains. These lines are crossed in order to have the tissue-specific gene knockout in those mice that inherit both the floxed gene and the Cre-expressing transgene. The Cre mice expresses the Cre ("creates") recombinase under the control of a promoter that is specific for a particular cell or tissue type. The lox-P ("locus of crossover P1") contains a targeted gene flanked by two loxP sites ("floxed gene") in a direct orientation. When the Cre recombinase is expressed, the deoxyribonucleic acid (DNA) segment flanked by the loxP sites is excised and consequently inactivated. Contrarily, when the Cre recombinase is not expressed, the gene flanked by loxP sites remains active. Cre recombinase is an enzyme that recognizes specifically loxP sites and catalyzes DNA recombination between these [45].

In the Cre/loxP system, promotor activation of Cre recombinase leads to permanent activation of a reporter gene. If the Cre enzyme is fused to the estrogen receptor (ER), an additional control of reporter activation will be achieved, because this fusion prevents the nuclear localization of Cre-ER proteins. The expression is spatially and temporally controlled by the administration of an estrogen analog (such as tamoxifen) as, after binding to Cre-ER, there is a translocation of the recombinase into the nucleus, where it recombines with the loxP site [46,47].

The Cre/loxP recombinase system can be also used for activation of gene expression. Lineage ablation allows the investigation of cell function, so the transgenic expression of diphtheria toxin receptor (DTR) to turn diphtheria toxin (DT)-resistant mouse cells into DT-sensitive cells was developed as a strategy of inducible lineage ablation. In 2005, Buch *et al.* developed a Cre-inducible DTR (iDTR) transgenic mice, in which Cre-mediated excision of a STOP cassette turns cells sensitive to DT (Figure 1.3) [48]. This mouse allows to study *in vivo* cell lineage ablation after application of DT that has an effect only in tissues or cells expressing DTR.

To generate the iDTR transgenic mouse, the DTR transgene had to be placed under the control of a ubiquitously expressed promoter to allow DTR expression in various cell types upon Cre-mediated excision of a STOP cassette. The promoter corresponding to this feature was Gt(Rosa)26Sor locus (also known as Rosa26). Thus, a loxP-flanked STOP cassette and the open reading frame (ORF) of DTR (as DTR is not endogenously expressed in mice) was introduced into the aforementioned locus. Cre recombinase allowed DTR gene expression, so DT-mediated ablation of specific target cells was achieved. The few limitations of this method are the expression strength and pattern of the Gt(Rosa)26Sor promoter that will determine the presence of DTR and the deletion frequency of the STOP cassette achieved by the specific Cre strain [48].

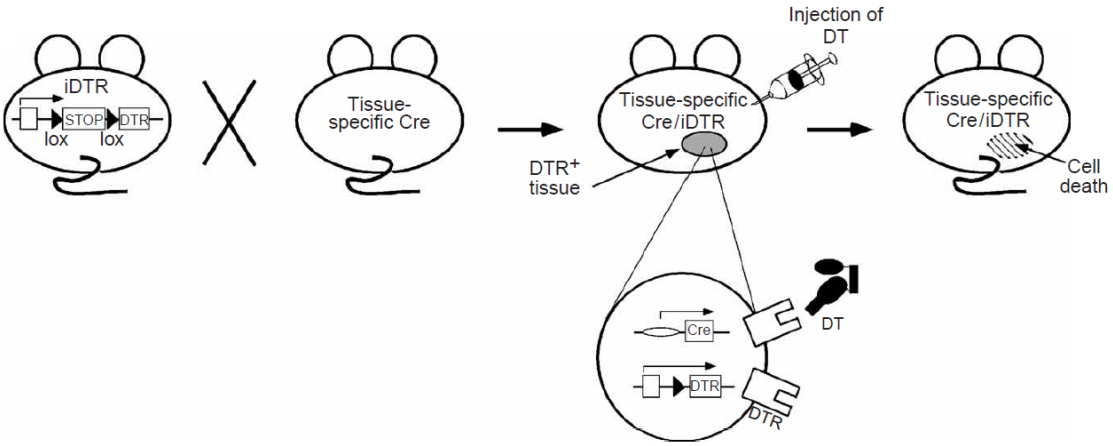

Figure 1.3 – Schematic representation of TH-Cre; LSL-DTR mice [48].

Myelin loss after DT injections was observed in a MOGi-Cre/iDTR, which expresses Cre recombinase under the control of the oligodendrocyte-specific promoter of the gene encoding the myelin oligodendrocyte glycoprotein (MOG). This shows that DT crosses the blood-brain barrier (BBB) and promotes cell ablation in the CNS. Therefore, iDTR cell ablation system is a valuable tool to study the function of both peripheral and CNS cells [48].

To achieve the ablation of peripheral and CNS cells, DT has to be administered to mice expressing DTR. DT was purified, crystallized, and characterized in many laboratories and the first publication of its crystal structure occurred in 1992 (Figure 1.4) [49–51]. DT was described in the culture medium of *Corynebacterium diphtheriae*, being naturally excreted by strains of diphtheria bacilli and it is toxic for many species such as man, guinea pigs, rabbits, and some birds, but animals like rats and mice are resistant to DT [49,51,52].

DT, a protein of 58,342.0 Da, is a single polypeptide chain, containing 535 aminoacids that, after proteolytic cleavage (with trypsin, pronase or “natural proteases”), can split into two distinct fragments, connected through a disulfide bond. Fragment A, with a molecular mass of 21,167.0 Da, is enzymatically active, while the carboxyl-terminal fragment B (37,195.0 Da) is needed for attachment of toxin to cells and to facilitate the delivery of fragment A to the cytosol [49–53]. Fragment A is highly stable with little loss of activity when heated at 100 ^{o}C or rapidly exposed to pH values between 2 and 12; fragment B promptly denatures and precipitates after dissociation from fragment A [49,51,52].

DT has three functional and structural domains implicated in cell intoxication:

- The enzymatic or catalytic (C) domain – corresponding to the first 193 amino acids residues (hydrophobic N-terminal) of fragment A, that is inserted into the plasma membrane. It is responsible for the nicotinamide adenine dinucleotide (NAD)-dependent adenosine diphosphate (ADP)-ribosylation of elongation factor 2 (EF-2), resulting in inhibition of protein synthesis in the cytosol. Therefore, EF-2 was shown to be DT target and substrate;

- The receptor-binding (R) domain - located at the hydrophilic C-terminal (residues 389 to 535), of fragment B and responsible for recognition and interaction with specific surface receptors on sensitive targeted cell membranes. The binding to the receptor allows toxin internalization into acidic intracellular compartments;

- The transmembranar or translocation (T) domain - localized in the fragment B (residues 200 to 379) and responsible for the internalization of domain C of DT to the cytoplasm by membrane penetration [49–53].

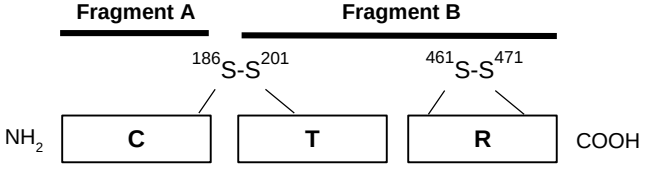

Figure 1.4 – Representation of DT structure (adapted from 50).

The DT mechanism of action has been studied extensively [53]. The mechanisms of enzymatic activity, receptor binding, and receptor mediated endocytosis are known in detail, but mechanisms for C domain translocation and release of an active enzyme into the cytosol are not known yet [50–52].

The effect of DT on protein synthesis was first described during respiration studies on HeLa cells by the observation of protein accumulation [49]. DT enters cells via receptor-mediated endocytosis. The R domain binds to specific cell-surface receptors and C domain (fragment A) is internalized into endosomes, leaving fragment B outside of the cell [50–53].

For its biological properties, DT is now being exploited to design new biotechnological tools and therapeutics. Also the engineering of proteins with therapeutic value using the properties of DT is being developed. One of the ideas under development consists in using DT as a way of translocate proteins other than the C domain of DT into cells. DT was the first engineered bacterial toxin to reach the market (FDA-approved therapy for lymphomas) and it is expected that, in the future, useful biotechnological and medical applications of DT will reach the market [50].

A TH-Cre mice have the TH promotor directing the expression of Cre recombinase to catecholaminergic cells, so central and peripheral nervous systems are ablated, when DT is administered to TH-Cre; LSL-DTR mice. Thus, to achieve ablation of SNS without affecting CNS, a strategy to avoid DT in the brain is needed. This strategy involves protein modification in such a way that it does not cross the BBB (Figure 1.5).

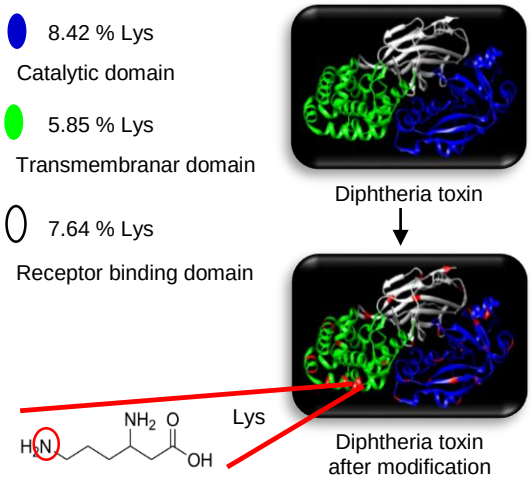

Figure 1.5 – Strategy to avoid DT in the brain.

1.6. Protein modifications

The use of proteins as therapeutics agents has been expanded in the last years as a result of discovery of novel proteins, better understanding of their mechanism of action, improvements in expression, and discovery of molecule-altering technologies that have the ability to deliver polypeptides *in vivo* [54]. Proteins are now used to diagnostic, monitor and treat several diseases, but parenteral administration possess disadvantages that limit their usefulness. Some of these limitations are: short circulating half-lives, low solubility, immunogenicity, susceptibility to proteolytic enzymes destruction, and rapid clearance. This implies that several administrations are needed for the drug to be effective, leading to cost increase and higher risk of adverse reactions [54–56].

Chemical reactions are now used to site-selective modify proteins of interest and overcome the aforementioned disadvantages [57]. Different strategies have been employed, such as manipulation of amino acid sequence, conjugation to immunoglobulins and serum proteins, incorporation into drug delivery vehicles and conjugating to natural or synthetic polymers [54,57]. The major concern in these modifications is the possible occurrence of structural modifications and thus different functions [58].

The process of covalent linking one or more polyethylene glycol (PEG) chains to modify a protein, peptide or non-peptide molecule, leaving a N-hydroxysuccinimide (NHS) group, is called PEGylation (Figure 1.6) [56,58–62]. In 1977, Davis and Abuchowski performed first PEGylation reaction in albumin and catalase [55,58–60]. Nowadays, it is a well-established, widely

employed and fast growing technology that overcomes safety and efficiency requirements of drugs [59]. PEGylation is considered a protein modification methodology to improve biomedical efficacy, bioactivity and physicochemical properties, for instance, of pharmacological agents [54,59,61]. It was used in several therapeutic molecules, such as peptides, proteins, antibodies, antibody fragments, oligonucleotides, small drugs, cofactors, lipids, and saccharides [56,60,63].

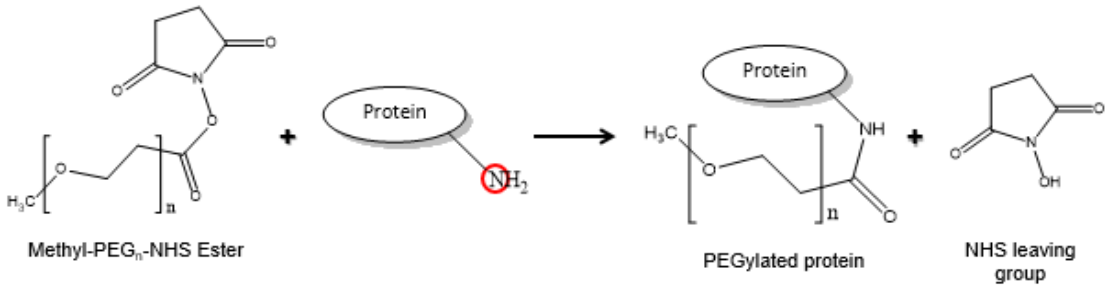

Figure 1.6 – Representation of a general PEGylation reaction (adapted from 54).

PEG is formed by the link of repeating units of ethylene glycol to form polymers with different molecular masses and usually its reactive electrophilic functional group is attached to a specific site of the molecule of interest. In most cases, protein amines (nucleophilic groups) are used as conjugation sites: Ɛ-amino groups of lysines and the N-terminus of polypeptide molecules (α-amino group). However, the sulfhydryl group of cysteine residues is also widely used [54–56,58–61,63,64]. Lysines are polar and relatively abundant amino acids residues usually located on the protein surface, which make them prone to chemical reactions with PEG reagents [59].

PEG is a biocompatible polymer that offers several advantages, such as being nontoxic, non-immunogenic, non-antigenic and highly soluble in water. It is a FDA-approved compound that has been used as an excipient in many pharmaceutical and cosmetic formulations [55,56,58–60,63,65,66]. PEG-drug conjugates also present advantages such as a prolonged plasma circulation in the body, decreased protein immunogenicity, and a decreased degradation by metabolic enzymes [55,56,58–60,62–67]. The PEG to protein ratio used in the PEGylation reaction determines the reaction yield and the number of attached PEGs to a protein [61]. Properties of PEG-drug conjugates depend on: the number of PEG chains attached to the drug, structure and shape of PEG used, the location of the PEG sites on the polypeptide, and the chemistry used to attach PEG [54–56,59,61].

PEG polymer attached to a protein increases its hydrodynamic radius, thus reducing renal filtration. In addition, PEG shields the protein from proteases degradation and immune system recognition. It also increases water solubility, which turns conjugates more polar and renders BBB crossing more difficult [54–56,60,62–65].

PEGylation is one of the most successful strategies to improve the delivery of therapeutic molecules [55,60]. The first PEGylated product, PEG-adenosine deaminase (PEGylated form of adenosine deaminase), was FDA-approved, in 1990, to treat severe combined immunodeficiency (SCID). After that, at least eight PEGylated peptide and protein conjugates have been approved as therapeutic agents [56,58–61,63,65–67]. Some examples are PEG-asparaginase (to treat acute lymphoblastic leukemia), PEGylated fragment antigen-binding (Fab) fragment of tumor necrosis factor (TNF) inhibitor monoclonal antibody (mAb) (to treat Crohn's disease and rheumatoid arthritis), PEG-granulocyte colony stimulating factor (to stimulate the proliferation, differentiation and survival of neutrophils that are depleted during chemotherapy) [56,58–60,62,65]. Apart from approved drugs, more PEGylated products that are now in clinical trials are expected to be in the market in the next years. The use of successful different PEGylated products is an indication of their usefulness, efficacy and safety [54,55,58–60].

Another approach to modify proteins includes taking advantage of the conjugation between serum albumin and α-maleimide (Mal)-functional polymers (Figure 1.7) [68]. This strategy allows the increase in size of DT, in order to minimize clearance. Nevertheless, it was also reported that maleimidation technique leads to heterogeneous mixtures and may result in denaturation [69].

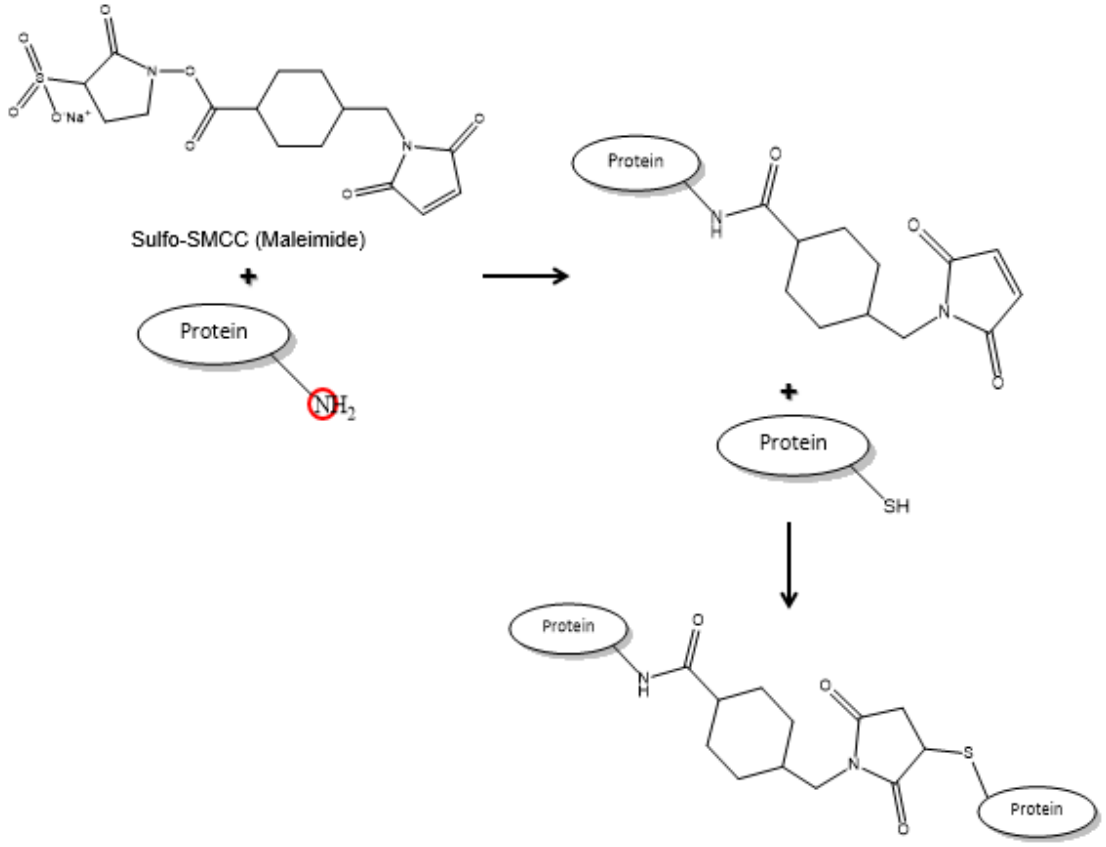

Figure 1.7 – Representation of a general maleimidation reaction (adapted from 68).

2. Materials and Methods

2.1. DT modification

1 mg of DT unnicked, *Corynebacterium diphtheriae* (Calbiochem, #322326) was reconstituted in 1 mL of conjugation phosphate buffered saline (PBS) 1X (concentration 16 µM). PBS 1X was prepared by Instituto Gulbenkian de Ciência (IGC) services and is constituted by 137 mM sodium chloride, 2.7 mM potassium chloride, 10 mM sodium phosphate and 2 mM potassium phosphate. Both modifications were performed using 80 equivalents of modifying agent in relation to DT. Hence, 0.001269 mmol of each crosslinker were needed.

PEGylation: $MS(PEG)_4$ methyl-PEG-NHS-Ester (Life Technologies, #22341), after being fully equilibrated to room temperature (RT), was reconstituted in 1.1 mL of dimethyl sulfoxide (DMSO, Sigma-Aldrich, #D8418), leading to a concentration of 250 mM PEG, according to manufacturer instructions. 250 mM PEG was diluted 1:100 in DMSO and then the appropriate volume was transferred into DT solution. The mixture was incubated for 4 h, at RT, under shaking. Reaction to produce PEGylated DT (PEGyDT) was monitored by electrophoresis of samples collected every hour (see electrophoresis section).

Maleimidation using sulfosuccinimidyl 4-(N-maleimidomethyl)cyclohexane-1-carboxylate (sulfo-SMCC): 1.5 mg of sulfo-SMCC (Life Technologies, #22322) were dissolved in 272.7 µL of ultra-pure water. The appropriate volume was then dispensed into DT solution. Reaction to generate DT Mal occurred for 4 h, at RT, under shaking. Every hour a sample was taken to be accessed by electrophoresis (see electrophoresis section).

Purification of PEGyDT and DT Mal: In order to remove the excess of cross-linker, gel filtration chromatography using the gravity protocol of PD MidiTrapG-25 column (GE Healthcare, #28-9180-08) was performed according to manufacturer indications. Briefly, column was prepared and equilibrated with buffer. Sample was applied to the column, the flow-through was discarded and eluate was collected.

***In vitro* DT Mal and bovine serum albumin (BSA) conjugation:** 1 mg/mL of BSA fraction V (NZYtech, #MB04601) was added to DT Mal. DT Mal BSA was produced by incubation for 30 min, under shaking, at RT.

Concentration determination: The concentrations of PEGyDT, DT Mal and DT Mal BSA were determined using a NanoDrop ND-2000 UV-Visible spectrophotometer (Fisher Scientific, #11840301), measuring the absorbance at 280 nm of 1 µL-samples and using PBS buffer as blank.

2.2. Sodium dodecyl sulfate polyacrylamide gel electrophoresis (SDS-PAGE)

All the materials needed to perform the experiment described in this section were kindly provided by Alekos Athanasiadis' lab (special acknowledgment to Krzysztof Kus). 10 µL of each sample were mixed with 1X diluted NuPAGE LDS Sample Buffer 4X (Life Techonologies, #NP0007). The mixtures were boiled at 90 ^{o}C, for 3 min. 10 µL of Novex Sharp Unstained Protein Standard (Life Technologies, #LC5801) and 15 µL of each sample were applied in a gel NuPAGE Novex 12 % Bis-Tris Protein Gels, 1.0 mm, 15 well (Life Technologies, #NP0343BOX). Separation occurred at 200 V, for around 1 h with running buffer 1X diluted NuPAGE MOPS SDS Running Buffer 20X (Life Technologies, #NP0001). The gel was washed with water for 5 min, 3 times and stained for 20 min with SimplyBlue SafeStain (Life Technologies, #LC6060). After staining, gel was washed with water, shaking (2 days).

2.3. Mass spectrometry (MS)

DT, PEGyDT and DT Mal samples were analyzed by matrix-assisted laser desorption / ionization – time of flight (MALDI-TOF) at the Protein & Nucleic Acid Chemistry (PNAC) Facility, Department of Biochemistry Sanger Building, University of Cambridge. Samples were previously concentrated in Amicon Ultra-2, Ultracel-10 membranes (Sigma-Aldrich, #Z740164)

prepared according to manufacturer instructions (centrifuged for 4 min, 3500 *g*, with PBS 1X). DT, PEGyDT and DT Mal were centrifuged 3500 *g* until appropriate concentration (10 µM).

2.4. Cell culture of HeLa cells

HeLa cells (a human cell line) were kindly provided by Lars Jansen's lab (special acknowledgment to João Mata). Cells were maintained in Dulbecco's modified Eagle medium (DMEM) high glucose with L-glutamine and sodium pyruvate (Biowest, #L0104) supplemented with 10 % fetal bovine serum (FBS) heat inactivated (Biowest, #S181BH) and 1 % penicillin-streptomycin (Biowest, #L0022-100) – DMEM complete medium. Cells were maintained in humidified atmosphere, 5 % CO_2 at 37 ^oC. To maintain cells in culture: first, a wash with PBS 1X was done, then 1 to 3 mL TrypLE Express Enzyme 1X, phenol red (Life Technologies, #12605) were applied and the cells were incubated for 5 min, in humidified atmosphere, 5 % CO_2 at 37 ^oC. To inactivate TrypLE, 5 mL of DMEM complete medium was added and the cells were centrifuged for 5 min, 300 *g*, at RT. Finally, cells were resuspended in 5 mL of DMEM complete medium and plated in a cell culture flask (Corning, #CORN430825). Cells were plated in Costar 12 and 24 Well Clear TC-Treated Multiple Well Plates (Corning, #3513 and #3526) following a procedure similar to the one used to maintain cells, but after centrifugation and resuspension, the cells were counted in a hemocytometer (Neubauer Cell with Double Grid, Fisher Scientific, #10350141) using 1 % Trypan Blue solution (Sigma-Aldrich, #T8154). 10^5 cells per well (2 mL/well) and $6x10^4$ cells per well (1 mL/well) were plated in the Costar 12 and 24 plates, respectively.

DT concentration test: Three different concentrations of DT were tested: 1 µg/mL, 3 µg/mL and 5 µg/mL and controls without DT were used. Fluorescence-activated cell sorting (FACS) analysis (for details see FACSCalibur analysis section) was done at 4 h, 6 h, 12 h, 24 h and 48 h. For 1 µg/mL, also 72 h was analyzed.

DT, PEGyDT, DT Mal and DT Mal BSA: All incubations used a concentration of 3 µg/mL (except controls, in which only medium was added). The time points were prepared at 4 h, 6 h, 12 h, 24 h, 48 h and 72 h.

BSA: This assay was done to prove that DT Mal would be the responsible for HeLa cell death and not BSA. Therefore, 2.25 mg/mL were incubated for 24 h, 48 h and 72 h.

FACSCalibur analysis: Samples were prepared for analysis in a Becton Dickinson Flow Cytometer FACSCalibur. Data were acquired using CellQuest software (Becton Dickinson) and analyzed using FlowJo. The medium was collected and cells were washed with PBS 1X, 250 to 500 µL of TrypLE were added and incubated in humidified atmosphere, 5 % CO_2 at 37 ^oC. DMEM complete medium (250 to 400 µL) were added and cells were centrifuged for 4 min, 3250 *g*, at 4 ^oC. Cells were resuspended in 150 µL FACS buffer (2 % FBS, 0.02 % sodium azide-1-^{15}N (Sigma-Aldrich, #609374) in PBS 1X) and 25 µL propidium iodide (Sigma-Aldrich, #P4170) were added. The medium collected before preparation procedures was also analyzed.

2.5. Bone marrow (BM)-derived macrophages from Rosa26Cre-ER(T2); LSL-DTR mice

Tamoxifen (Hefei Joye) was administered *in vivo* to Rosa26Cre-ER(T2); LSL-DTR mice and, after 1 month, the BM cells were isolated to be differentiated *in vitro* into primary macrophages. The back legs of aforementioned mice were cleaned and the BM cells inside the bone were flushed into a Petri dish (Nunc, #150318) with DMEM high glucose with L-glutamine and sodium pyruvate cell culture medium. After homogenization, cells were centrifuged for 5 min, 300 *g*, at RT. Cells were resuspended and maintained in Iscove's modified Dulbecco's medium (IMDM) GlutaMAX (Life Technologies, #31980-022) supplemented with 10 % FBS; 1 % penicillin-streptomycin; 0.1 % 2-mercaptoethanol (Life Technologies, #31350-010); 0.5 % sodium pyruvate (Life Technologies, #11360-070) – IMDM complete medium. To stimulate differentiation, 30 % macrophage colony stimulating factor (M-CSF) (kindly provided by Elsa Seixas) was added to the medium. Petri dishes were incubated in humidified atmosphere, 5 % CO_2 at 37 ^oC for 7 days. After differentiation, the macrophages were harvested and centrifuged for 5 min, 300 *g*, at RT. Cells were resuspended in 10 mL IMDM complete medium and counted

in a hemocytometer using trypan blue, as previously described. $5x10^5$ cells were plated per well (1 mL/well) in a Costar 24 Well Clear TC-Treated Multiple Well Plate.

Tamoxifen *in vivo*: A stock solution of tamoxifen at 20 mg/mL in corn oil (Sigma-Aldrich, #C8267) was prepared and homogenized by shaking, at 37 ºC for 2 to 3 h. To have a final concentration of 1 mg/mL, a dilution of the stock solution was done in corn oil. An intraperitoneal (i.p.) injection of 50 µL was given, in milky spot, to Rosa26Cre-ER(T2); LSL-DTR pups that were one day older for 5 to 6 consecutive days.

DT and PEGyDT: 3 µg/mL of DT and PEGyDT were prepared in IMDM complete medium. FACSCalibur analysis was performed at 4 h, 6 h, 12 h and 24 h.

FACSCalibur analysis: Macrophages were harvested and then centrifuged for 4 min, 3250 *g*, at 4 ºC. FACSCalibur analysis was performed as previously described (see Cell culture of HeLa cells section for details).

2.6. Mice and housing conditions

Mice were housed at controlled temperature and humidity, under a 12 h light/dark cycle. Food and water were supplied *ad libitum*, except if something different is mentioned. The animals were euthanized using carbon dioxide. All procedures were approved by IGC ethical committee. All controls were injected with vehicle (PBS 1X). C57BL/6 mice were obtained from the Mice Production Facility at IGC. TH-Cre (#008601) and LSL-DTR (#007900) mice were purchased from Jackson Laboratory. LSL-DsRed mice was imported from Rockefeller University. Rosa26Cre-ER(T2) animals were kindly provided by Miguel Soares' lab (special acknowledgment to Sílvia Cardoso and Sofia Rebelo).

2.7. PEGyDT-mediated sympathectomy

TH-Cre; LSL-DTR mice were used for this experiment and LSL-DTR, C57BL/6 and TH-Cre mice were used as controls. During the experiment, animals and food were weighted every day. Both DT and PEGyDT were injected i.p.. Injections of 25 ng/g of DT or PEGyDT were administered once a day for 8 consecutive days. TH-Cre; LSL-DTR mice were also injected i.p. with PBS 1X for 8 consecutive days. During the experiment, animals and food were also weighted every day.

Assessment of SNS ablation by confocal microscopy: Mice were perfused with PBS 1X followed by 4 % formaldehyde (VWR, #9713.9010). The brain was removed and fixed in 4 % formaldehyde for 2 days, at 4 ºC. Using a vibratome VT 1000S (Leica), 50 µm thick slices of ventral tegmental area (VTA) were obtained. These slices were at RT for 1 h, shaking in blocking buffer (1 % BSA, 0.1 % tween 20 (Sigma-Aldrich, #P2287), 0.05 % sodium azide in PBS 1X). The slices were incubated with primary antibody TH chicken (1:1000, Aves Lab, #TYH) o/n, shaking, at 4 ºC. After washing, secondary antibody Alexa Fluor 594 Goat Anti-chicken IgY (H+L) (1:500, Life Technologies, #A-11042) was applied for 1 h, shaking, at RT. After secondary antibody incubation, slices were washed and mounted with Dapi-Fluoromount-G (Southern Biotech, #0100). The microscope slides were dried at RT and then kept at 4 ºC.

Fibers isolated from inguinal fat were fixed in 2 % formaldehyde for 2 h, at RT, shaking. After blocking for 1 h, at RT, fibers were incubated with primary antibodies rabbit polyclonal to neuron specific β_3-Tubulin (β_3-Tub) (1:1000, Abcam, #AB18207) and TH chicken, o/n, shaking, at 4 ºC. After washing, secondary antibodies Alexa Fluor 488 Goat Anti-rabbit IgG (H+L) (1:500, Life Technologies, #A-11008) and Alexa Fluor 594 Goat Anti-chicken were applied for 1 h, shaking, at RT. After secondary antibodies incubation, fibers were washed and mounted with Fluoromount-G. The microscope slides were dried at RT and then kept at 4 ºC.

Confocal images were acquired in Leica TCS SP5 Inverted and Upright Microscopes. Analysis and quantification of acquired images was performed using FIJI [70].

Scoring test: After administration of 25 ng/g of DT or PEGyDT once a day for 8 consecutive days, movies of mice were done. These movies were presented to people strange to the experiment (to assure that a blind test was performed), but used to work with mice model. The question "How many animals are moving normally?" was asked.

2.8. Functional tests on sympathetic ablated mice

From this point forward, TH-Cre; LSL-DTR strain was used as experimental mice and LSL-DTR strain was used as control mice (unless something else is specified).

Fasting: Food was taken out from the cages and mice were weighted every 12 h during 48 h. After this period, food *ad libitum* was provided to mice.

High Fat Diet (HFD) studies: Animals were weighted and normal diet (ND) was replaced by HFD. Mice were weighted every week during 4 weeks and photographs were taken. C57BL/6 animals that were on HFD for 4 weeks were weighted. HFD (ssniff, #E15742-347) contains 60 kJ % fat.

Yo-yo diet (HFD - ND - HFD - ND) and food intake: HFD was replaced by a ND regimen, then animals were fed with HFD followed by another period of ND. During this period, mice were weighted and food intake was measured.

BMI: Nose-to-anal distance was measured and mice were weighted to calculate the BMI. This measurement was performed in ND and HFD regimens.

HFD 2 weeks after sympathectomy and food intake: ND was replaced by HFD 2 weeks after sympathectomy was performed. Mice weight and food intake were measured every day.

Fasting glucose and Glucose Tolerance Test (GTT): After 12 h fasting during dark cycle, glucose was measured using Accu-Chek Aviva Glucose (Roche Diagnostics, #05987431023) and the mice were weighted. After this, an i.p. injection of 2 mg/g D-(+)-glucose (Sigma-Aldrich, #G8270) was administered and glucose level was measured at 15 min, 30 min, 60 min, 90 min, 120 min and 150 min post-injection. These procedures were performed in ND and repeated for 5 weeks in HFD regimen.

Fasting insulin: Blood samples were collected using heparin (LEO Pharmaceutical Products, #0014425-02) after a dark cycle with no access to food. Samples were centrifuged for 15 min, 9400 *g*, at 4 ^{o}C and plasma was collected. Centrifugation was repeated once. Mouse Ultrasensitive Insulin Enzyme-Linked Immunosorbent Assay (ELISA) (ALPCO #80-INSMSU) was used to measure insulin and the protocol was followed according to manufacturer instructions. These procedures were performed in ND and repeated after 5 weeks in HFD regimen.

Cold exposure: Body temperature was measured using an electronic thermometer ama-digit ad 15 th (Precision, #E910 560) when the animals were housed at RT and animals were weighted. After this, animals were housed at 4 ^{o}C with ND food and water *ad libitum*. Body temperature was measured and animals were weighted every hour for 8 h.

2.9. Anti-obesity drugs

Fen hydrochloride (Sigma-Aldrich, #F8507) and AMPH hydrochloride (Asiba Pharmatech, #10296-HCl) were used to induce sympathetic activation. Unless stated otherwise, C57BL/6 animals were used and food and water were provided *ad libitum*. Controls were administered with vehicle (PBS 1X).

Fen: Mini-osmotic pumps Model 2004 (Alzet, #298) releasing 6 mg/kg/day of Fen hydrochloride or PBS 1X were implanted. For surgery procedures, mice were anesthetized with isoflurane (Fluka/Sigma-Aldrich, #Y0000858) and Anesthesia system AutoFlow System (E-Z Anesthesia, #EZ-AF9000) was used. Animals and food were weighted every other day. Mini-osmotic pumps Model 2004 with PBS 1X were also implanted in animals that were pair-fed to the ones in Fen hydrochloride treatment (pair-fed animals have access to the same amount of food that was eaten by mice in Fen hydrochloride treatment). After 28 days, osmotic pumps were removed (same surgical procedures as described previously) and weight and food intake measurements were done for 28 days. These procedures were performed on mice that were in HFD.

AMPH: AMPH hydrochloride was prepared every day. Mice on HFD were injected i.p. with AMPH hydrochloride 20 mg/kg every day during 7 weeks. Animals that were pair-fed to the ones on AMPH hydrochloride were injected with PBS 1X. Animals and food were weighted every day. After ceasing AMPH administration, mice and food were weighted during 4 weeks.

TH-Cre; LSL-DTR (after sympathetic ablation) and LSL-DTR mice on HFD received an i.p. injection of AMPH hydrochloride 20 mg/kg, every day during 4 weeks. Another group of TH-Cre; LSL-DTR (after sympathetic ablation) and LSL-DTR mice on HFD received an i.p. injection of PBS 1X, every day during 4 weeks. Animals and food were weighted every day.

2.10. OPT

As stated before, this technique was applied to characterize fat and to show its innervation.

Organ dissection and preparation: C57BL/6 mice were perfused with PBS 1X and after that, inguinal and epididymal fats were carefully removed (with Dumont #5 Forceps) and cleaned. Fats were fixed in 4 % formaldehyde for 3 h, under shaking, at RT. Then, fats were washed and placed in a 1 % agarose, low gelling temperature (Sigma-Aldrich, #A9414) at RT, protected from dust. The agarose volume was approximately 24.5 cm^3 (3.5 cm height and 1.5 cm diameter).

Clearing: Fats inside agarose were immersed in 10 % methanol p.a. Normapur (VWR, #VWRC2084.307) for 2 h, at RT, under shaking. Afterwards, 10 % increasing steps were performed every day until dehydration in 100 % methanol was reached (RT with agitation). The replacement of the methanol with 1:2 mixture of benzyl alcohol (Merck Millipore, #822259) and benzyl benzoate (Merck Millipore, #818701) was performed in 15 % increasing steps every day until clarification was reached. Photographs were taken before and after clearing and measurements of fats were done.

OPT acquisition and analysis: OPT acquisition was performed by Gabriel Martins and Ânia Gonçalves from Unit of Imaging and Citometry (UIC) of IGC. Briefly, images of the whole fat tissue were acquired using a 1X lens, mounted on an Infinitube tube lens, and projected into a Hamamatsu FlashLT sCMOS camera. A total of 1600 images were acquired for a full rotation (0.25 ^{o} steps). The series of projections were then pre-processed using FIJI [70] in order to remove hot pixels, re-align the axis of rotation in relation to the camera-chip, and finally the back-projection reconstruction was done using the Skyscan's nrecon software. The stack of slices was further processed with FIJI, to increase contrast and saved to posterior analysis with the software Amira V5.3. Using Amira V5.3, 3D reconstructions and image segmentation were performed to identify and reconstruct individual parts of the fat organs.

2.11. Statistical analysis

All the statistical analyses were performed in Sigma Plot 11.0, using One-Way ANOVA test. A P value < 0.05 was considered as statistically significant. Data were represented as mean ± standard error of the mean (SEM).

3. Results

3.1. PEG and Mal bind to DT

DT modification state was analyzed by SDS-PAGE and by MS. SDS-PAGE shows that after gel filtration chromatography a slight increase in molecular weight (MW) is present both in PEGyDT and in DT Mal. When DT Mal is attached to BSA the shift is even higher (Figure 3.1 A).

By MS technique, it is possible to see that between 1 and 5 PEG molecules were attached to DT and that around 15 Mal molecules were attached to DT (Figure 3.1 B and C). The attachment of 1 molecule of PEG or Mal increases DT MW by 218 g/mol. Thus, the attachment of 5 PEG molecules increases DT MW by 1,090.0 g/mol and the attachment of 15 Mal molecules increases DT MW by 3,270.0 g/mol.

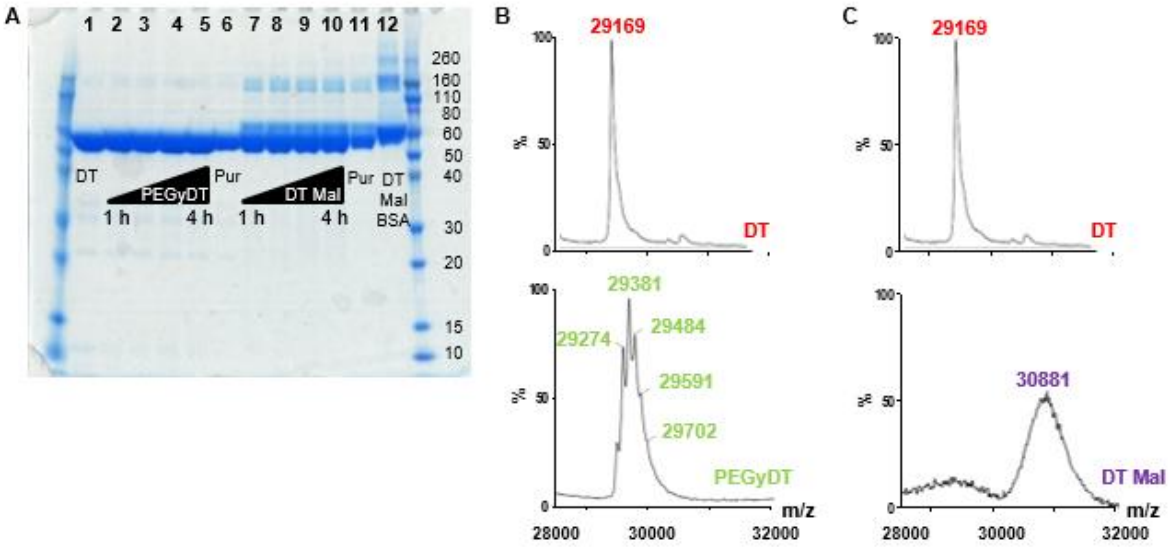

Figure 3.1 – Assessment of DT modification state. A) SDS-PAGE. 1 – DT; 2-5 – PEGyDT after 1 h, 2 h, 3 h and 4 h of reaction, respectively; 6 – PEGyDT after purification; 7-10 – DT Mal after 1 h, 2 h, 3 h and 4 h of reaction, respectively; 11 – DT Mal after purification; 12 – DT Mal after incubation with BSA; MW marker is in both sides of the gel and MW is indicated on the right side; B) MS of DT (top) and PEGyDT (bottom) samples. DT peak is identified in red and PEGyDT peaks are identified in green; C) MS of DT (top) and DT Mal (bottom) samples. DT peak is identified in red and DT Mal peak is identified in purple.

3.2. PEGyDT, but not DT Mal, remains functional after modification

First, a DT concentration test was performed to determine the concentration that should be used to cause cell death in HeLa cells (Figure 7.1 in Appendix). Although 1 µg/mL of DT was enough to cause 100 % cell death, to further test DT and its modified derivatives 3 µg/mL was used.

FACS analysis was performed to access DT and its modified derivatives capacity to cause cell death. After 24 h, DT and PEGyDT already induce around 50 % of cell death, while after 48 h or more, the cell death is almost 100 % (*** $p < 0.0001$). The same did not happen with DT Mal and DT Mal BSA that did not present a significant difference from control (Figure 3.2).

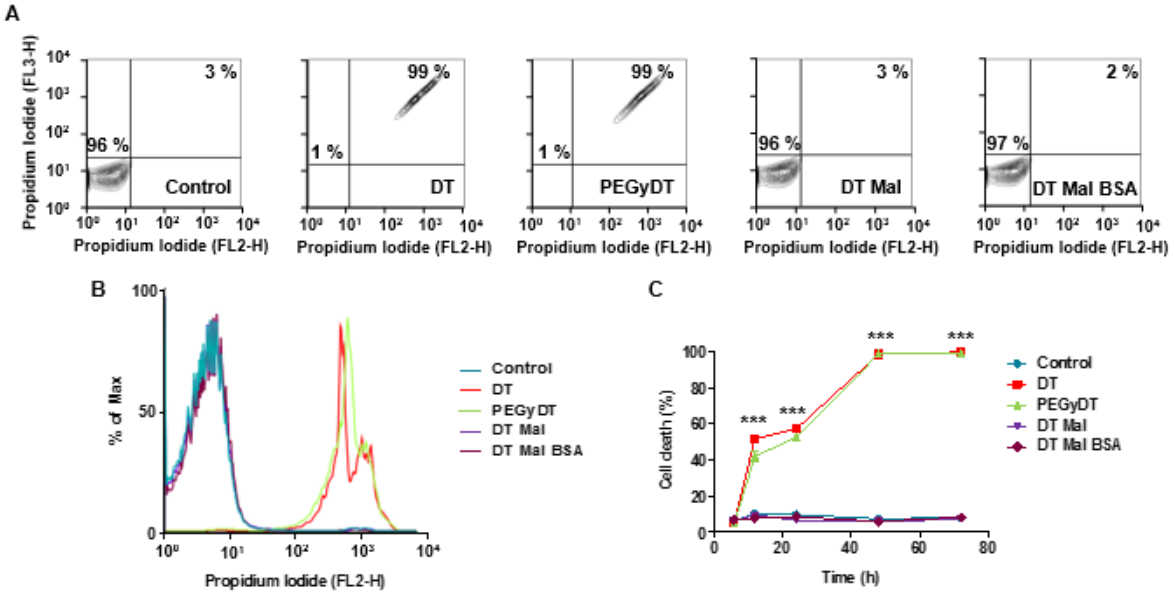

Figure 3.2 – DT functionality after modification tested on *in vitro* HeLa cell line culture. A) Representative contour plots of Control, DT and PEGyDT, DT Mal and DT Mal BSA populations after 48 h of incubation in HeLa cells; B) Representation of live and dead cell populations after 48 h of incubation with DT, PEGyDT, DT Mal and DT Mal BSA in HeLa cells; C) Quantification of HeLa cell death during time after incubation with DT, PEGyDT, DT Mal and DT Mal BSA (*** $p < 0.0001$, $n = 3$). Data are represented as mean ± SEM (Figure 7.2 in Appendix).

To demonstrate that BSA was not responsible for the obtained results in cell culture when Mal was tested an experiment was performed (Figure 7.3 in Appendix). The results indicate that BSA does not cause cell death of HeLa cells. As consequence, in case DT Mal would cause cell death, this would be exclusively a consequence of DT maleimidation and not to the presence of BSA.

Also primary cells were used to confirm the results obtained for the cell line (Figure 3.3). The primary cells used were BM-derived macrophages from Rosa26Cre-ER(T2); LSL-DTR mice, to whom tamoxifen was administered. Although the cell death was higher than expected in control, in the presence of DT and PEGyDT it was significantly higher (*** $p < 0.0001$).

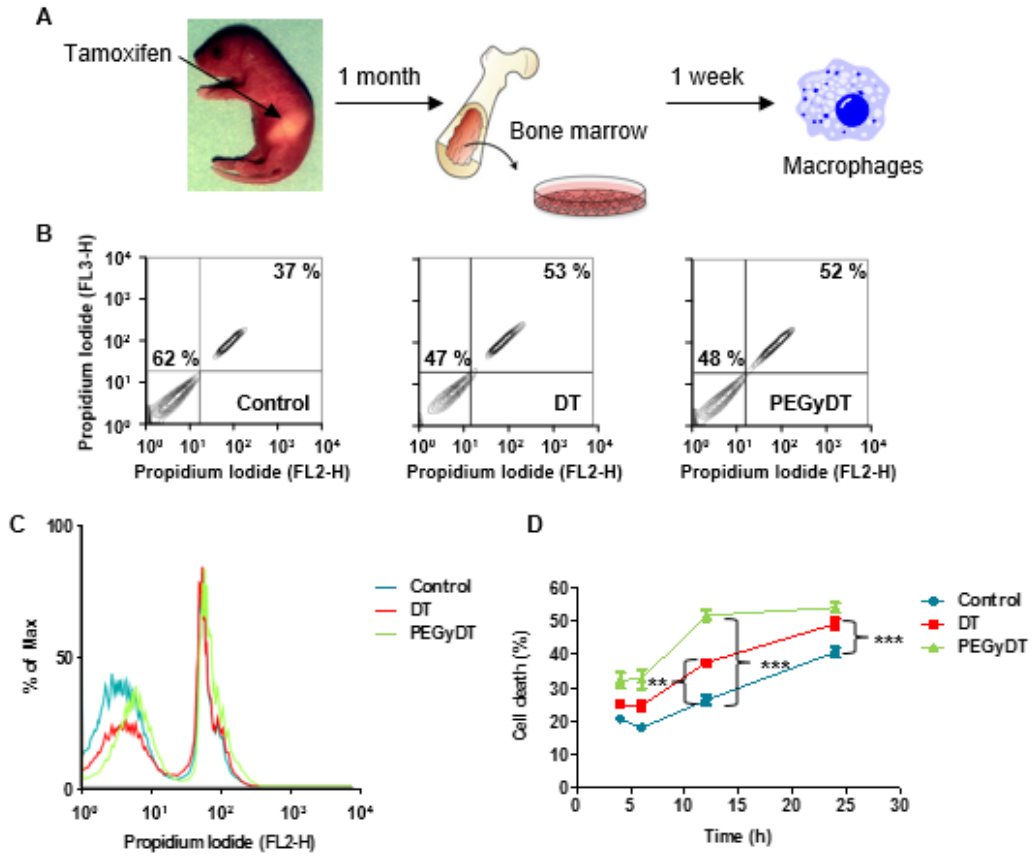

Figure 3.3 – DT functionality after modification tested *in vitro* on primary cell culture of macrophages derived from the BM of Rosa26Cre-ER(T2); LSL-DTR mice after tamoxifen was administered *in vivo*. A) Schematic representation of the experiment; B) Representative contour plots of Control, DT and PEGyDT populations after 24 h of incubation in macrophages; C) Representation of live and dead cells populations after 24 h of incubation with DT and PEGyDT in macrophages; D) Quantification of macrophage death during time after incubation with DT and PEGyDT (** $p < 0.001$, *** $p < 0.0001$, $n = 3$). Data are represented as mean ± SEM (Figure 7.4 in Appendix).

3.3. PEGyDT does not kill catecholaminergic neurons in the brain, but it kills sympathetic nerves

The weight of TH-Cre; LSL-DTR mice was reduced from 27 g to 23 g (* $p < 0.01$) when injected with DT (Figure 3.4 A), but a weight reduction was not verified when PEGyDT was injected (Figure 3.4 B). Also the food intake was reduced from 3 g/day to only 1 g/day (** $p < 0.001$) when DT was administered to mice (Figure 3.4 C). Again, this decrease was not seen when PEGyDT was injected (Figure 3.4 D). Weight variation and food intake were also measured in TH-Cre; LSL-DTR that were administered with PBS (Figure 7.5 in Appendix) and no fluctuations were verified.

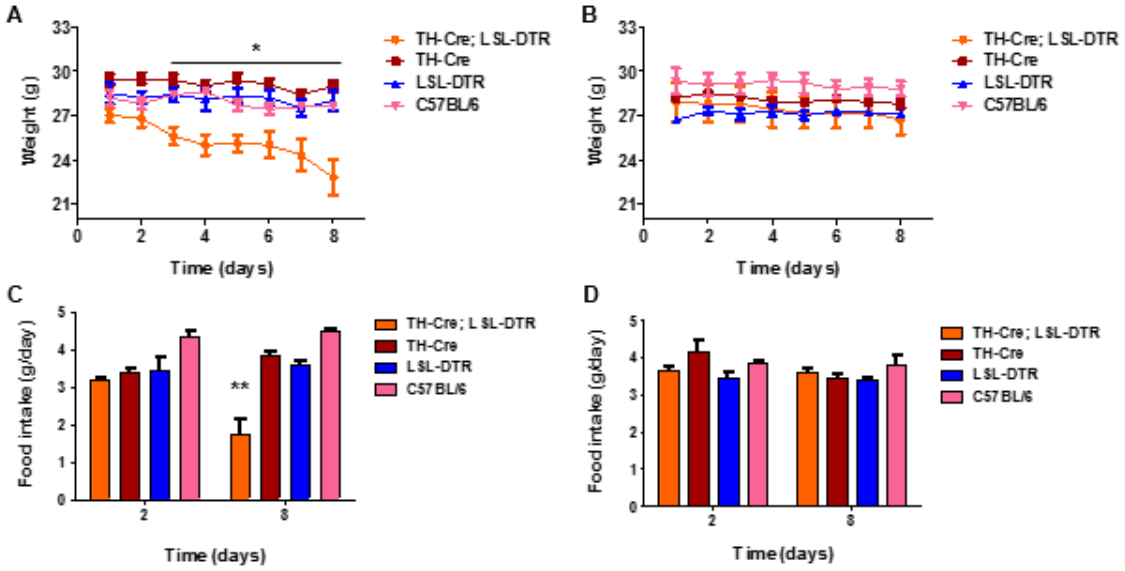

Figure 3.4 – Differences in weight and in food intake between TH-Cre; LSL-DTR mice injected with DT and PEGyDT. A) Mice weight during daily administration of 25 ng/g of DT (* $p < 0.01$, n = 3-4); B) Mice weight during daily administration of 25 ng/g of PEGyDT (n = 3-5); C) Food intake on the first and last day of administration of 25 ng/g of DT (** $p < 0.001$, n = 3-4); D) Food intake on the first and last day of administration of 25 ng/g of PEGyDT (n = 3-5). Data are represented as mean ± SEM.

A scoring test was also performed and it was clear to people strange to the experiment that mice injected with DT lose the capacity to move normally, while mice to whom PEGyDT was administered have no alterations in locomotion (Figure 7.6 in Appendix).

Mice were sacrificed to analyze the presence of TH in brain and in fibers from inguinal fat. As expected, TH / 4',6-diamidino-2-phenylindole (Dapi) ratio in the brain of mice to whom DT was administered is lower than 10 % (** $p < 0.001$), while in the brain of mice that were injected PEGyDT this ratio is 50 % (Figure 3.5 A and B). These results suggest that PEGyDT does not kill catecholaminergic neurons in the brain.

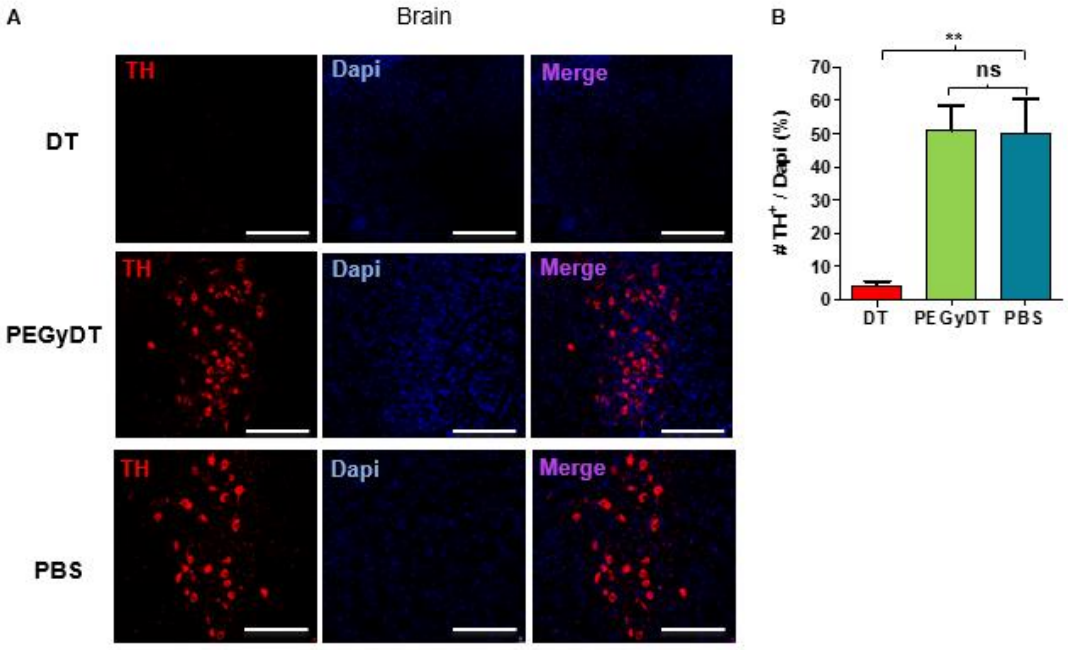

Figure 3.5 – PEGyDT does not kill catecholaminergic neurons in the brain. A) Confocal microscopy imaging of VTA stained for TH neurons after *in vivo* injection of DT, PEGyDT or PBS. Scale bar is 250 µm (n = 12); B) Quantification of TH^+ / Dapi neurons after *in vivo* injection of DT, PEGyDT or PBS (** $p < 0.001$, n = 3). Data are represented as mean ± SEM.

The presence of TH in the fibers is also important to reveal the action of PEGyDT in sympathetic neurons (Figure 3.6 A and B). The results obtained show that DT and PEGyDT have a similar capacity to reduce the ratio of TH / β_3-Tub to less than 20 % (*** $p < 0.0001$).

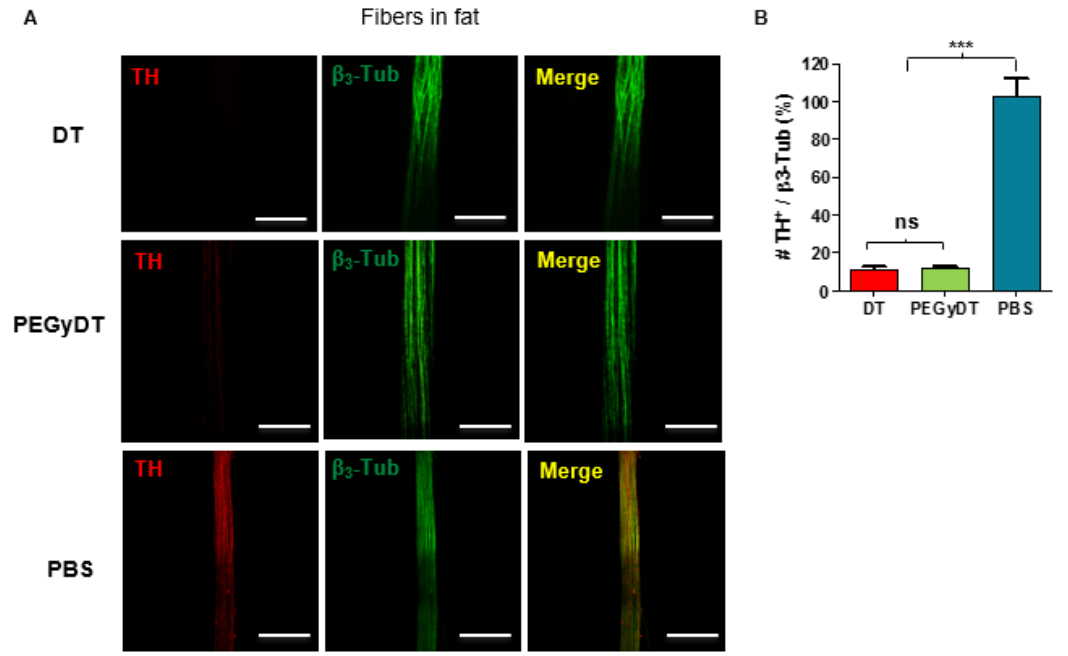

Figure 3.6 – PEGyDT kills sympathetic nerves. A) Confocal microscopy imaging of fibers obtained from fat and stained for TH neurons and for β_3-Tub after *in vivo* injection of DT, PEGyDT or PBS. Scale bar is 100 µm (n = 12); B) Quantification of TH^+ / β_3-Tub neurons after *in vivo* injection of DT, PEGyDT or PBS (*** $p < 0.0001$, n = 3). Data are represented as mean ± SEM.

3.4. Sympathectomy leads to irreversible obesity, without changing food intake

Fasting of TH-Cre; LSL-DTR and LSL-DTR mice for 48 h does not reveal differences between each other in weight loss (Figure 3.7 A).

HFD leads to a significantly higher (*** $p < 0.0001$) increase in weight of sympathectomized mice: TH-Cre; LSL-DTR mice weight is around 40 g after 4 weeks in HFD, while LSL-DTR mice weight is around 20 g after the same period in HFD (Figure 3.7 B). This is already an indication that the speed of weight gain is also significantly higher (** $p < 0.001$) for TH-Cre; LSL-DTR mice (Figure 3.7 C and D). While controls gain 10 g/month, TH-Cre; LSL-DTR mice gain more than two-fold (25 g/month) in body weight.

In C57BL/6 animals (Figure 3.7 E), the weight increased 20 % after 4 weeks in HFD, while the weight of TH-Cre; LSL-DTR mice increased more than 100 % (** $p < 0.001$).

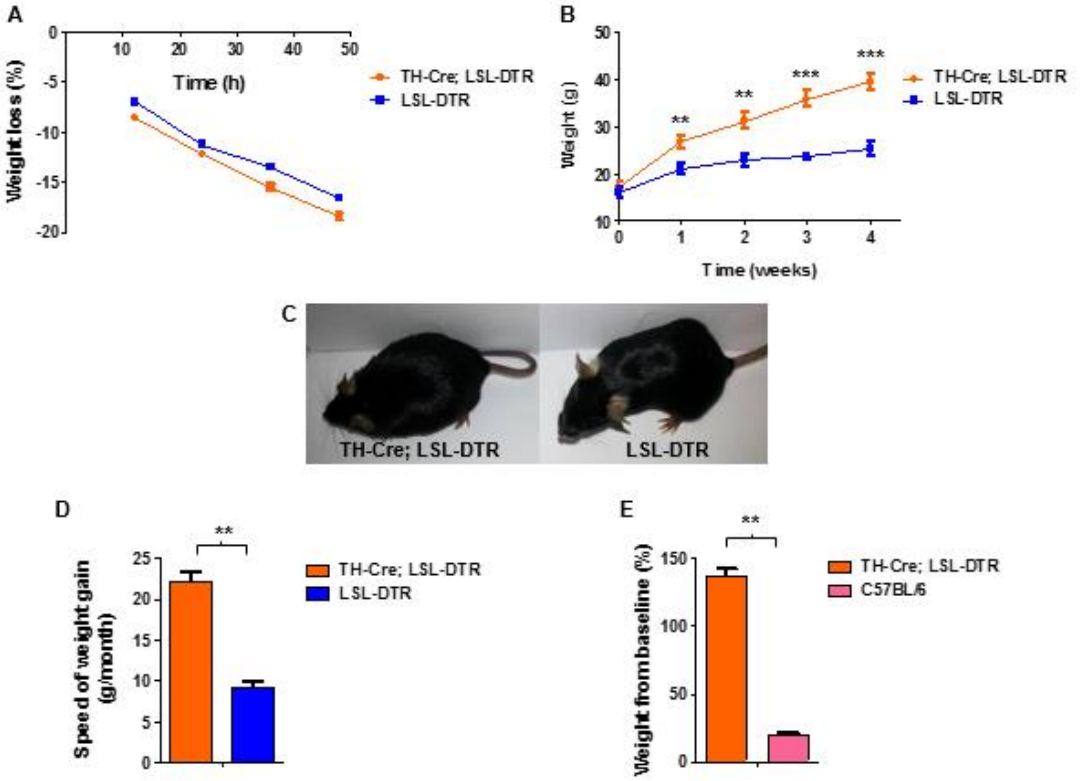

Figure 3.7 – Sympathectomy leads to obesity. A) Weight loss of TH-Cre; LSL-DTR mice during 48 h of fasting (n = 6); B) Weight gain during 4 weeks in HFD, after SNS ablation (** $p < 0.001$, *** $p < 0.0001$, n = 6); C)TH-Cre; LSL-DTR compared to LSL-DTR mice after 4 weeks of HFD regimen; D) Speed of weight gain during HFD regimen (** $p < 0.001$, n = 6); E) Comparison of weight gain between TH-Cre; LSL-DTR and C57BL/6 mice after 4 weeks in HFD (** $p < 0.001$, n = 5-10). Data are represented as mean ± SEM.

When the sympathectomized mice are presented to a yo-yo diet (alternating between HFD and ND), the diet-induced obesity is irreversible (Figure 3.8 A). The higher increase in weight and the inability to lose weight are more pronounced in the second period of HFD-ND (*** $p < 0.0001$).

It could be thought that these differences were caused by alterations in food intake, but this is not the case, as the food intake is 3 g/day for both experimental and control mice (Figure 3.8 B).

When in ND, TH-Cre; LSL-DTR mice present a similar BMI as the control strain (0.3 g/cm^2), but while in HFD the BMI of TH-Cre; LSL-DTR mice increase to almost 0.5 g/cm^2 (** $p < 0.001$). This is caused by the weight increase and not by the size increase (Figure 3.8 C).

The weight gain was also tested when mice were fed with HFD only 2 weeks after ablation of SNS (Figure 3.8 D). The data reveals that the differences in weight are the same as if mice were fed with HFD right after the ablation procedure (** $p < 0.001$). Food intake was also not different when HFD regimen was given to mice 2 weeks after ablation (Figure 7.7 in Appendix).

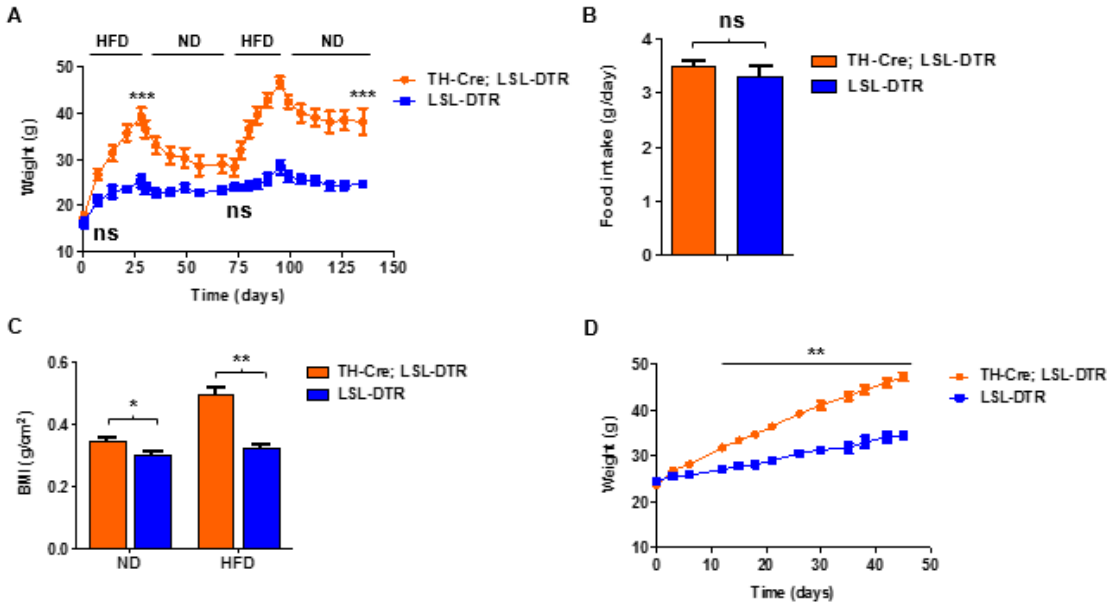

Figure 3.8 – Obesogenic effect of sympathectomy is irreversible and independent of food intake. A) Weight variation during a yo-yo diet (*** $p < 0.0001$, $n = 6$); B) Food intake during HFD feeding ($n = 6$); C) BMI in ND and in HFD (* $p < 0.01$, ** $p < 0.001$, $n = 48$ (ND), $n = 120$ (HFD)); D) Weight gain when HFD regimen starts 2 weeks after SNS ablation (** $p < 0.001$, $n = 5$-6). Data are represented as mean ± SEM.

3.5. Sympathectomy affects glucose tolerance, without affecting blood glucose and insulin

PEGyDT-mediated sympathectomized mice and LSL-DTR control mice were tested for several metabolic parameters when in ND and HFD regimen. The weight loss after 12 h of fasting was similar for experimental and for control mice. In ND regimen, mice lose around 6 % of weight, while in HFD this lost is reduced to 1 % of weight (Figure 3.9 A).

Even when in ND, glucose tolerance was affected in TH-Cre; LSL-DTR mice (** $p < 0.001$) suggesting that SNS has crucial role in glucose metabolism by adipose organs (Figure 3.9 B). Glucose tolerance of control mice was only affected after 5 weeks of HFD (Figure 3.9 C).

After fasting neither blood glucose nor blood insulin were affected by the ablation process, in both types of diet. Glucose before HFD was around 100 mg/dL and after HFD an increase to 150 mg/dL was observed. Insulin in ND was around 0.3 ng/mL and, after HFD, there was a decrease to 0.2 ng/mL, consistent with the glucose increase (Figure 3.9 D and E).

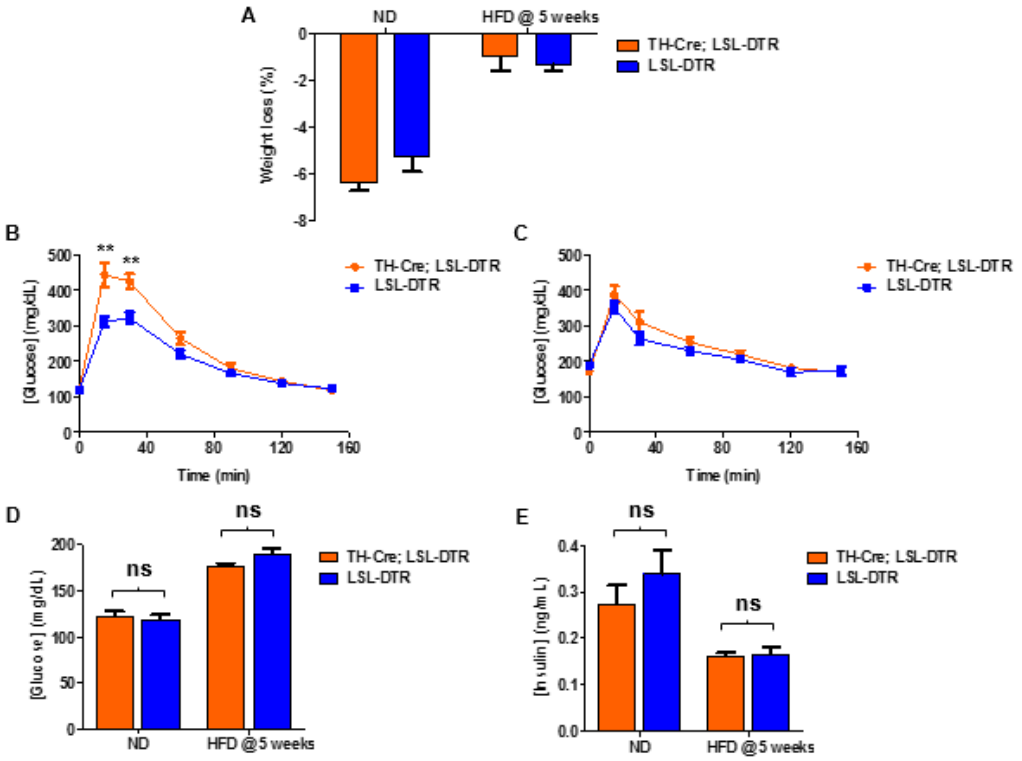

Figure 3.9 – Sympathectomy affects glucose tolerance, without affecting blood glucose and insulin. A) Body weight during the fasting period previous to GTT (n = 6-9); B) GTT during a ND feeding (** p < 0.001, n = 6-8); C) GTT after 5 weeks of HFD feeding (n = 6-9); D) Blood glucose concentration after 12 h of fasting for ND and HFD regimen (n = 6-8); E) Blood insulin after 12h of fasting concentration for ND and HFD regimen (n = 6-9). Data are represented as mean ± SEM.

3.6. Sympathectomy affects thermogenesis

When exposed to cold for 8 h both the sympathectomized TH-Cre; LSL-DTR strain and the control LSL-DTR strain present a similar weight loss around 5 % (Figure 3.10 A), but ablated mice were not able to maintain the body temperature (Figure 3.10 B). While control mice had a 2 ºC reduction (from 36 ºC to 34 ºC), ablated mice showed a two-fold higher decrease (*** p < 0.0001) in body temperature (from 36 ºC to 32 ºC).

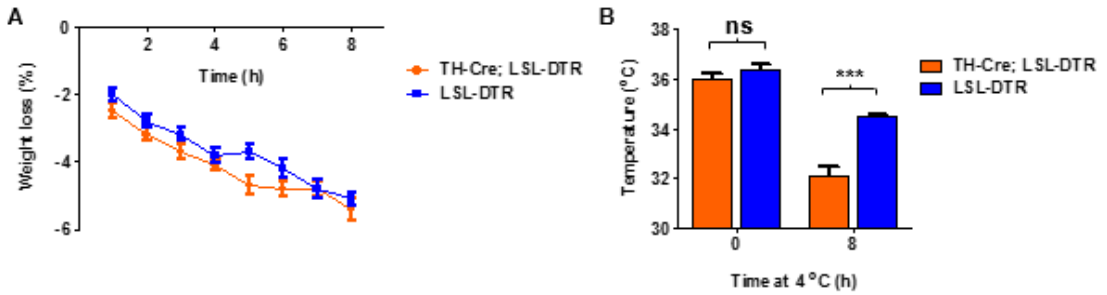

Figure 3.10 – Sympathectomy affects thermogenesis. A) Weight loss during cold (4 ºC) exposure (n = 5); B) Body temperature during cold (4 ºC) exposure (*** p < 0.0001, n = 5). Data are represented as mean ± SEM.

3.7. AMPH prevents obesity, independently of food intake

Prior to AMPH studies, a preliminary test was performed using Fen (Figure 7.8 in Appendix) in mice, to whom HFD food regimen was given. The results indicate a very slight difference (not significant) in weight while Fen was released and no differences in food intake were detected (while Fen was released and also after administration). After ceasing Fen administration, mice that were previously administered with the drug demonstrate a higher increase in weight. The absence of differences in food intake was the reason to use another sympathomimetic anti-obesity drug (AMPH) to promote SNS activation.

AMPH suppresses the appetite (Figure 3.11 A) and this is shown by the food intake reduction from 5 g/day to 3 g/day in C57BL/6 mice (** $p < 0.001$). Nevertheless, this is not the only effect (Figure 3.11 B) as animals that were pair-fed to the ones administered with AMPH have a greater increase in weight (* $p < 0.01$).

After ceasing AMPH administration, the food intake of C57BL/6 experimental mice returns to 5 g/day, which is similar to the food intake of C57BL/6 control mice (Figure 3.11 C). The mice that were previously administered with AMPH had an increase in weight of 34 % and the control group and an increase in weight of half (17 %), as shown in Figure 3.11 D (** $p < 0.001$).

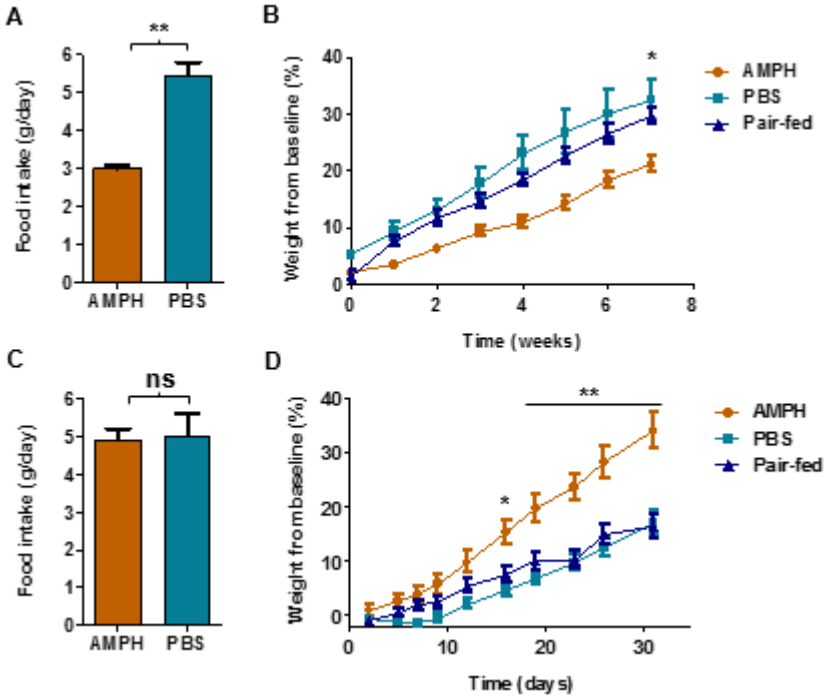

Figure 3.11 – AMPH prevents obesity, independently of food intake. A) Food intake during the period of AMPH administration (** $p < 0.001$, n = 96); B) Weight gain during the period of AMPH administration (* $p < 0.01$, n = 5-9); C) Food intake after ceasing AMPH administration (n = 30); D) Weight gain after ceasing AMPH administration (* $p < 0.01$, ** $p < 0.001$, n = 5-9). Data are represented as mean ± SEM.

3.8. SNS is required for AMPH effects

In vitro tests performed in the lab led to believe that the additional effect of AMPH could be related to the SNS (data not shown). To test this hypothesis, the difference in body weight between sympathectomized mice being administered with AMPH and PBS and non-sympathectomized mice being administered with AMPH and PBS was measured (Figure 3.12 A and B). The data show (Figure 3.12 C) that SNS is required for AMPH effects, as AMPH has a less pronounced effect in mice lacking SNS (** $p < 0.001$).

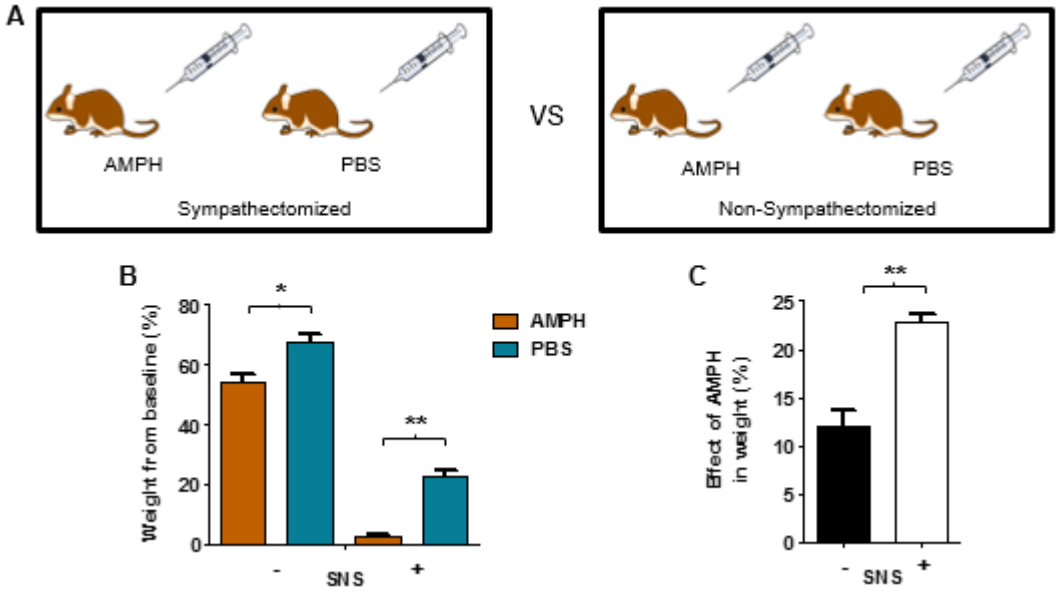

Figure 3.12 – SNS is required for AMPH effects. A) Schematic representation of the experiment; B) Weight gain of sympathectomized and non-sympathectomized mice administered with AMPH or vehicle (* $p < 0.01$, ** $p < 0.001$, n = 3-4); C) Effect of AMPH in weight in sympathectomized mice (** $p < 0.001$, n = 3-4). Data are represented as mean ± SEM.

3.9. OPT reveals neuroanatomy of inguinal and epididymal adipose organs

The differences between inguinal and epididymal fat depots, including intact structures within these fat organs, were visualized using OPT [71]. As it is shown in Figure 3.13, a rotating specimen placed in a cylinder of agarose gel is held in position for imaging. To reduce scattering, that occurs when the refractive index of the specimen is different from the refractive index of the medium, the sample is immersed in a 1:2 mixture of benzyl alcohol and benzyl benzoate (refractive index = 1.56).

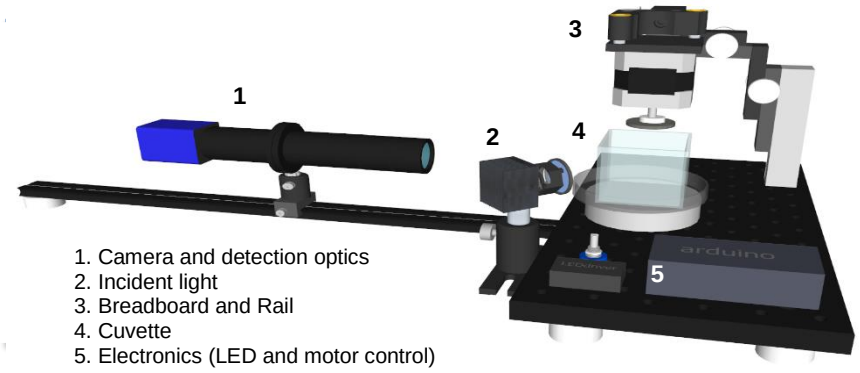

Figure 3.13 – Schematic representation of the OPT setup.

Before data acquisition, adipose organs were subject to a clearing technique (Figure 7.9 in Appendix). Image of raw data from the OPT of inguinal fat with 9 lines along the y axis (Figure 3.14 A) corresponding to 9 sinograms (Figure 3.14 B) represent the back-projection in the volumetric reconstruction of the OPT data.

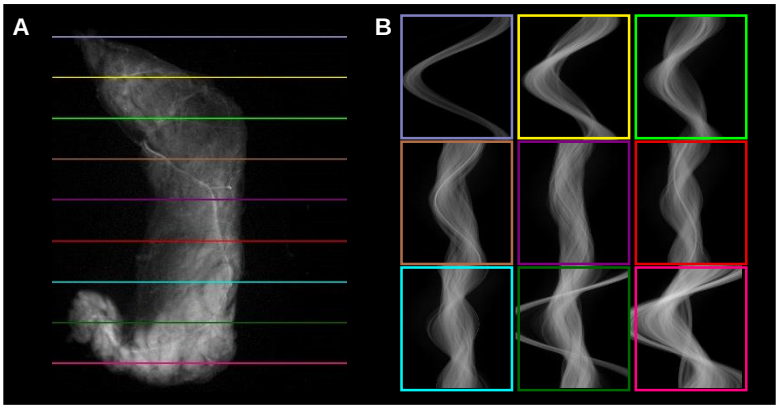

Figure 3.14 – Optical Projection Tomography (OPT) image acquisition and analysis. A) Raw data from the OPT of inguinal fat with 9 lines along the y axis corresponding to B) 9 sinograms.

OPT series of coronal sections of inguinal fat organ after 3D reconstruction are initially analyzed using FIJI software. Some of the structures present within the inguinal fat body, can be seen even without segmentation and tracing using Amira software (Figure 3.15 A). 3D reconstruction in maximal intensity projection (MIP) of the OPT coronal sections enables to visualize a rich network of vasculature present within the inguinal fat (Figure 3.15 B). The inguinal depot encloses the inguinal lymph node that is surrounded by abundant vasculature, as it is shown in orthogonal MIP of OPT slabs of inguinal fat (Figure 3.15 C).

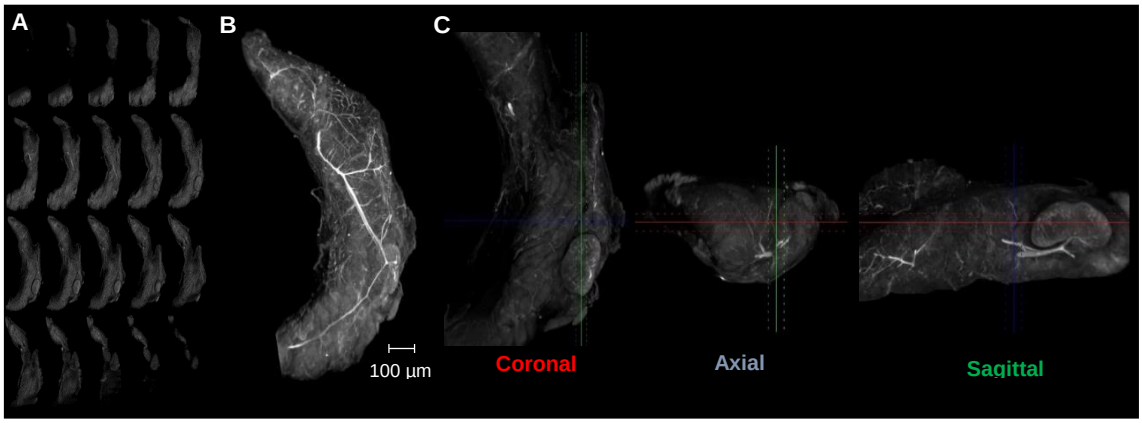

Figure 3.15 – OPT of inguinal fat. A) OPT series of coronal sections of inguinal fat organ after 3D reconstruction; B) 3D reconstruction in MIP of the OPT coronal sections; C) Orthogonal MIP of 450 µm OPT slabs of inguinal fat.

After image segmentation and tracing, it can be further noticed that vessels and nerve fibers (herein called paravascular nervi-vasorum), that are in proximity to the lymph node, run parallel to each other (Figure 3.16 A and B). It is also possible to distinguish individual nerve fibers in the superficial area of inguinal fat. The surface view of segmented structures enables to precisely follow the position of each of the segmented materials (Figure 3.16 C and D). As it can be seen in Figure 3.16 E, vessels and nerve fibers do not enter the lymph node.

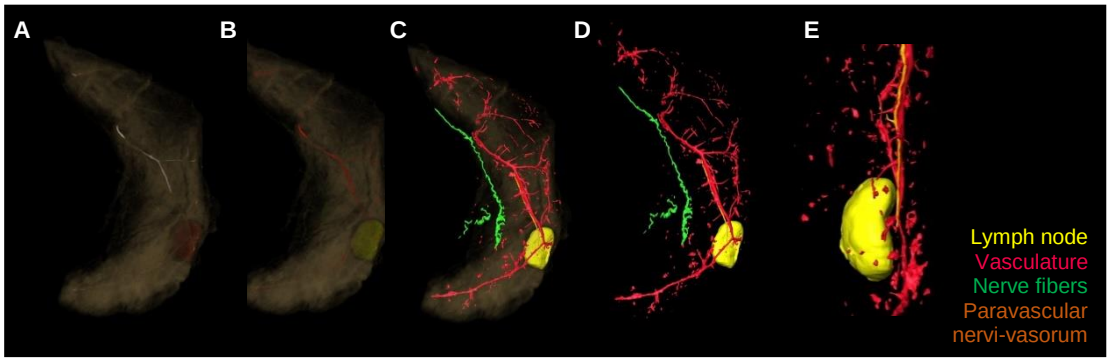

Figure 3.16 – Segmentation of structures within inguinal fat. A) Before segmentation; B) Segmentation of blood vessels (red), nerve fibers (green), paravascular nervi-vasorum (orange) and the lymph node (yellow); C) Surface view of segmented materials; D) Surface view of segmented materials without fat in the background display; E) Segmentation focused on vasculature and parivascular nervi-vasorum adjacent to the lymph node.

Inguinal fat depot is sub-compartmentalized in lobes (Figure 3.17 A and B), which merge to form morphologic units of various sizes (Figure 3.17 C).

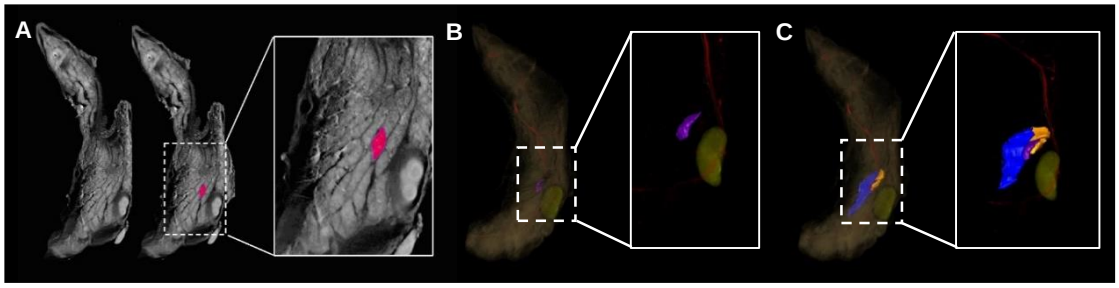

Figure 3.17 – Inguinal fat is sub-compartmentalized in lobes. A) Segmentation of an individual lobe (purple); B) 3D representation of an individual lobe; C) 3D representation of three independent lobes.

The epididymal fat occur in proximity to the testis and epididymis. OPT series of coronal sections were obtained after the 3D reconstruction of epididymal fat (Figure 3.18 A). Looking only at the 3D reconstruction in MIP and orthogonal MIP images of this organ, it is possible to see some of its structural details. Not only the presence of a vasculature network that is connected to the testis, but also the presence of granular substructures, a particular feature of the epididymal fat organ (Figure 3.18 B and C).

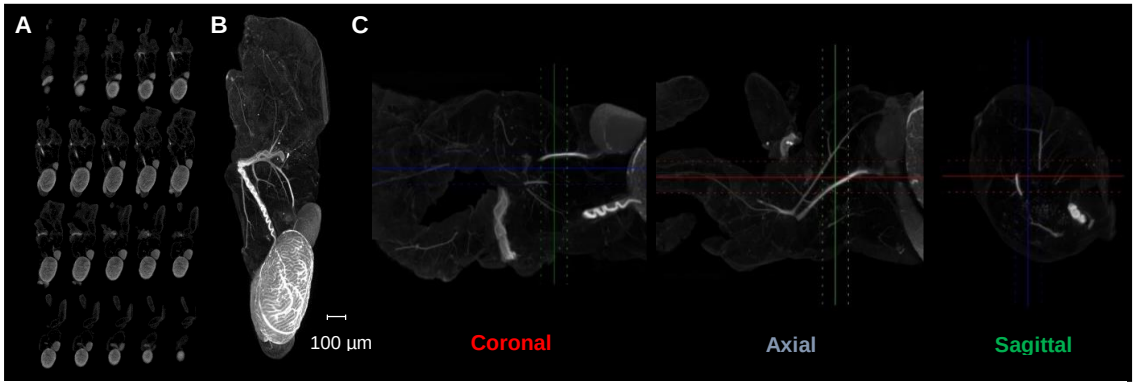

Figure 3.18 – OPT of epididymal fat. A) OPT series of coronal sections of epididymal fat organ after 3D reconstruction; B) 3D reconstruction in MIP of the OPT coronal sections; C) Orthogonal MIP of 1125 µm OPT slabs of epididymal fat.

The abundant vasculature is arising from the testis (testicular artery) and becomes more branched as it “spreads” throughout the epididymal fat, as it is shown in Figure 3.19 A and B. After segmentation and representation in surface view of the different materials present in epididymal fat organ, it is not detected the presence of lymph nodes, nor large nerve bundles as detected in the inguinal fat. The fat distribution is rather homogeneous (Figure 3.19 C and D).

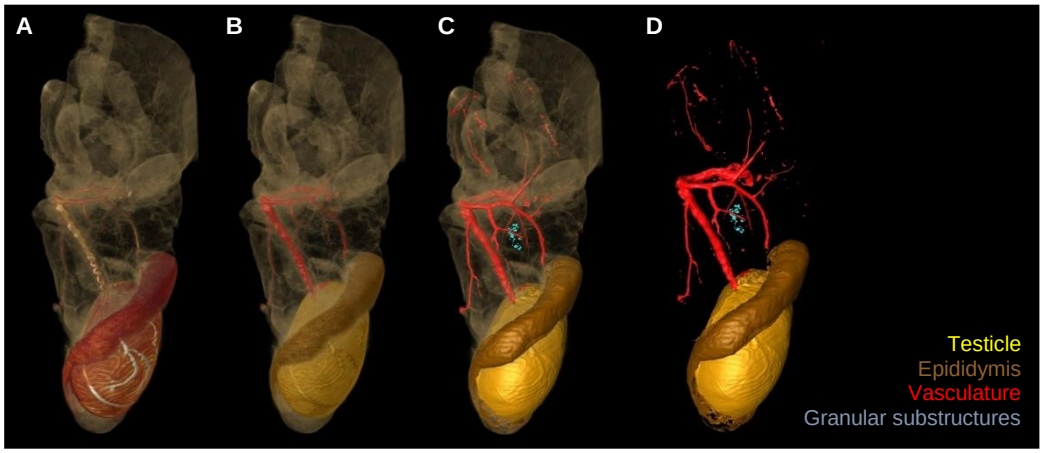

Figure 3.19 – Segmentation of structures within epididymal fat. A) Before segmentation; B) Segmentation of blood vessels (red), testicle (yellow), epididymis (brown) and granular substructures (blue); C) Surface view of segmented materials; D) Surface view of segmented materials without fat in the background display.

The presence of granular substructures within the epididymal fat organ was detected (Figure 3.20 A and B). These substructures are only present in a confined region within the epididymal fat organ and, interestingly, they are surrounded by vasculature (Figure 3.20 C).

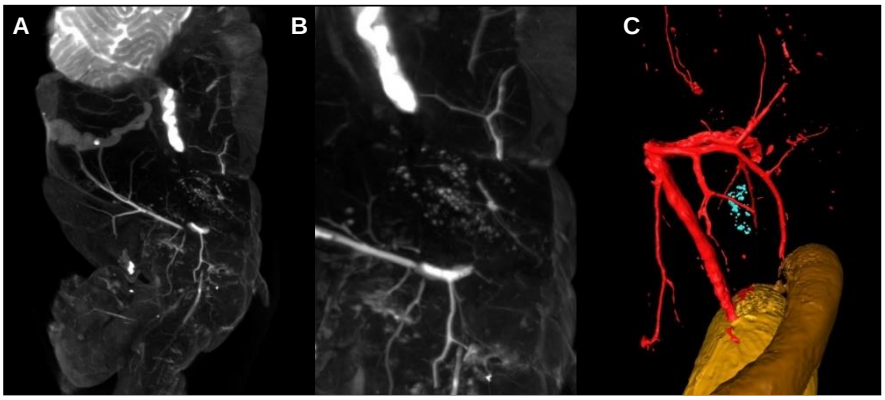

Figure 3.20 – Granular substructures confined to a region in epididymal fat. A) Reconstruction in MIP from the 3D stack obtained with OPT; B) Detailed view of the reconstruction in MIP from the 3D stack obtained with OPT; C) Surface view of segmented materials without fat in the background display: blood vessels (red), testicle (yellow), epididymis (brown) and granular substructures (blue).

Three graphical abstracts can summarize the findings of this work:

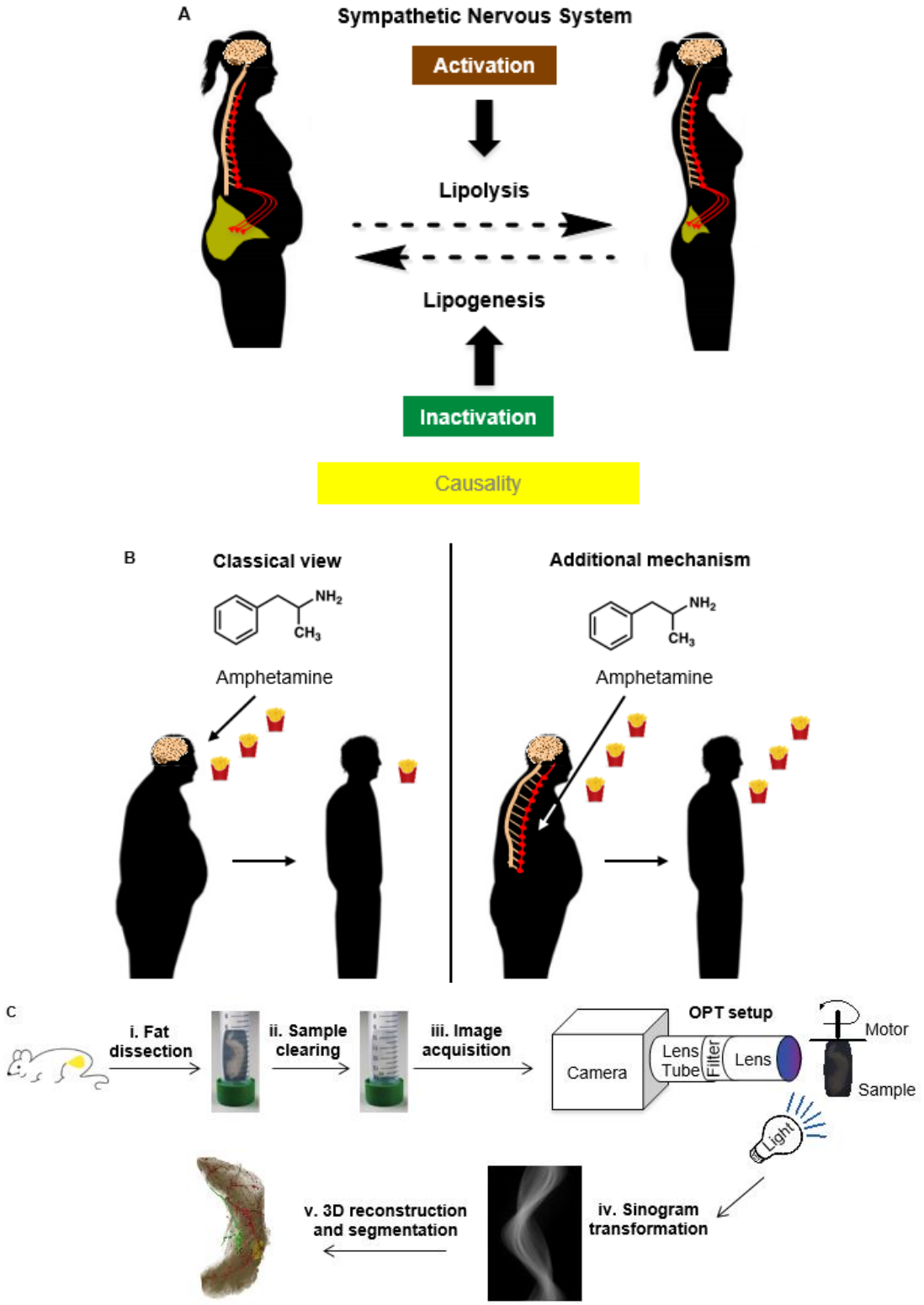

Figure 3.21 – Graphical abstracts summarizing the work. A) Demonstration of causality for MONA LISA hypothesis; B) Additional mechanism of action for AMPH; C) Neuroanatomy of adipose organs revealed by OPT.

4. Discussion

MONA LISA hypothesis states that obese people have a low sympathetic activity but its causality has never been shown. Are people obese because of low sympathetic activity or is the later just a consequence of obesity? This question remains. Experimental results that led to the MONA LISA hypothesis only measured NE reduction in the heart. Thus, there is no available data related to NE synthesis and to other sympathetic innervated organs.

One way to access causality of the MONA LISA hypothesis is to perform a loss of function of SNS and study the consequence of this action on body weight. This was achieved in this work after performing a PEGyDT-mediated sympathectomy in mice. The sympathectomy demonstrates that HFD causes an irreversible state of pronounced obesity, which is not caused by differences in food intake. Moreover, the blood glucose and insulin levels after a period of 12 h in food deprivation do not show differences between sympathectomized and non-sympathectomized mice, but the same is not true for a test that is not performed in a steady state (GTT), in which sympathectomized mice are intolerant to glucose while in a ND regimen. Furthermore, the results indicate that thermogenesis is impaired in ablated mice, thus these mice are not able to maintain their body temperature when exposed to a cold challenge.

In addition to a loss of function of SNS, it was probed its gain of function using AMPH. It was demonstrated that in addition to the brain effect that causes appetite suppression, also the SNS is required for the mechanism of action of AMPH.

To conclude this work, OPT coupled to tissue clearing was used to unravel the anatomy characterization of the inguinal and epididymal adipose organs. The results show that on one hand inguinal adipose organ contains a lymph node and is organized in a lobe-like structure and on the other hand, epididymal adipose organ does not contain lymph node, nor lobe structures. The different functions performed by these organs could be responsible by the anatomical differences but further studies should be performed to clearly understand this hypothesis.

SDS-PAGE showed a slight increase, after purification process, in MW both in PEGyDT and in DT Mal (Figure 3.1 A). As expected, the increase in MW is more pronounced in DT Mal BSA as this conjugate has more 66.5 kDa in its MW in result of BSA binding to Mal. All protein bands are present between 50 to 60 kDa, which is in accordance with DT MW (58 kDa). In DT Mal samples, it is possible to see faint bands around 160 kDa that could be a conjugate with more Mal molecules associated with DT.

Nevertheless, SDS-PAGE technique is only qualitative, so it does not allow to quantify the number of molecules from the modifying agent that were bound to DT. Therefore, MS was performed and using this technique, it was possible to demonstrate that when PEG was used, DT increased its MW between 218 g/mol and 1,090.0 g/mol (Figure 3.1 B). When Mal was used, the increase of DT MW was 3,270.0 g/mol (Figure 3.1 C). These results indicate that both PEG and Mal were linked to DT. The lower number of PEG molecules attached to DT is not a concern as the goal of this modification is to increase DT hydrodynamic radius, shield it from proteases and also make DT more polar, so that PEGyDT is less prone to cross the BBB.

After the modification process, the major concern was the functionality of the protein. Therefore, HeLa human cell line, endogenously expressing the DTR, was cultured *in vitro* and FACS analysis was performed in order to access cell death. First, a concentration test was performed and the results indicate that all the tested concentrations (1 µg/mL, 3 µg/mL and 5 µg/mL) were enough to cause 100 % of cell death after 48 h of incubation with DT (Figure 7.1 in Appendix). After knowing the concentration to be used, DT and modified derivatives were tested in a concentration of 3 µg/mL. It was demonstrated that, on one hand, DT and PEGyDT were able to kill 100 % of cells after 48 h of incubation, but on the other hand, the same killing capacity did not happen with DT Mal and with DT Mal BSA, even after a longer period of incubation (72 h). This could be explained with the loss of protein structure and, consequently loss of functionality, during the modification process. As reported, maleimidation can result in heterogeneous mixtures and also lead to protein denaturation [69]. PEGyDT had a maximum of 5 molecules attached, while DT Mal presented 15 sites of modification and this proved to be excessive to retain DT functionality.

To confirm the results obtained with the HeLa human cell line, another *in vitro* assay was performed, but this time using primary cells (BM-derived macrophages). Tamoxifen was first applied *in vitro* to macrophages derived from the BM of Rosa26Cre-ER(T2); LSL-DsRed mice and DsRed cells were not detected in FACS analysis and in confocal microscopy imaging (data not shown). This result was consistent even when different tamoxifen solvents (PBS,

ethanol and DMSO) were used. Therefore, the strategy was changed and tamoxifen was administered *in vivo* to Rosa26Cre-ER(T2); LSL-DTR mice and only after that, the BM cells were differentiated *in vitro* into macrophages. Cell death caused by DT and its modified derivative PEGyDT was significantly higher than the cell death present in control, in which no DT or PEGyDT was added. Cell death is not as high as in HeLa cells and this could be explained by the fact that DTR expression in macrophages is dependent on tamoxifen action. Although tamoxifen dose was previously optimized in the lab, this time the percentage of macrophages expressing DTR was not verified. Thus, it could be the case that DTR is not present in all the macrophages in culture and this explains the lower cell death, when compared to HeLa cell culture. The high cell death present in control samples can be explained with the high number of macrophages that were plated. This was caused by some problem with trypan blue during the process of cell counting that did not allow to count all the macrophages.

After *in vitro* verification of PEGyDT functionality, *in vivo* assays were performed. First, a dose optimization was performed in which different periods of administration of 10 ng/g, 25 ng/g and 50 ng/g were tested (data not shown). It was demonstrated that 25 ng/g of DT administered once a day for 8 consecutive days is enough to get a Parkinson-like phenotype and the same doses of PEGyDT do not have an effect on the phenotype (Figure 7.6 in Appendix). This result is already an indication that PEGyDT is not reaching catecholaminergic neurons in the brain and thus the CNS is not being affected as it is when DT is administered [48]. Apart from this, it was also observed that during DT administration, mice start to lose weight and to reduce their food intake (Figure 3.4 A and C), but with PEGyDT injections this is not observed (Figure 3.4 B and D). The reduction in food intake and the decrease in body weight while DT is administered is a result of the ablation of the CNS, as previously shown for the DT-treated MOGi-Cre/iDTR mice [48]. Mice that were administered with vehicle (PBS) had a similar response to those administered with PEGyDT (Figure 7.5 in Appendix) and this is again an indication that PEGyDT is not killing catecholaminergic neurons in the brain.

Despite the aforementioned indications about catecholaminergic neurons survival in the brain after PEGyDT administration, VTA from the brain and fibers from inguinal fat were fixed and stained to acquire images on confocal microscope (Figure 3.5 A and Figure 3.6 A). The results show that PEGyDT does not kill catecholaminergic neurons in the brain, while DT kills these neurons, as previously stated [48]. After quantification, it is possible to demonstrate that mice injected with PEGyDT have a ratio of TH to Dapi around 50 %, which is similar to the ratio obtained when PBS was administered (Figure 3.5 B). As DT kills catecholaminergic neurons, the aforementioned ratio is below 10 %. The analysis of fibers isolated from inguinal fat allowed to prove that the sympathetic neurons are ablated when PEGyDT is injected. This ablation is similar to the ablation obtained when DT is used. The ratio of TH to β_3-Tub is around 10 % for DT and its modified derivative PEGyDT, while when PBS is used this ratio is near 100 % (Figure 3.6 B).

In the aforementioned *in vivo* experiments, a method to specifically ablate the SNS was established, with no effect was detected on CNS. It is not possible to state that PEGyDT does not cross the BBB at all, however it is possible to prove that catecholaminergic neurons in the brain are not affected after PEGyDT administration. This was possible because after PEGylation, DT had a higher hydrodynamic radius, causing a lower renal filtration and it was protected from proteases. Moreover, after PEGylation DT became more polar, which hampers BBB crossing. This work allowed the development of a new tool to ablate SNS, the PEGyDT-mediated sympathectomy.

After being possible to perform the ablation of SNS, the next step was to unravel the effect of sympathectomy in weight control or, in other words, to understand the role of SNS in weight control by ablating it. The first test to be performed was to submit sympathectomized mice and non-sympathectomized control mice to a period of time with no access to food (fasting) (Figure 3.7 A). Hence, food was removed and no differences in terms of weight loss were seen between ablated and control mice during the 48 h of food deprivation. This result indicates that SNS is not, at least, a major regulator of weight control during a period of fasting. Nevertheless, SNS is deeply involved in weight control when a HFD regimen is given to mice, as ablated mice presented a much higher increase in weight (Figure 3.7 B). A significant difference in mice weight is observed just after one week in HFD, but only after 4 weeks in HFD is easily possible to see differences between experimental and control mice (Figure 3.7 C). This result leads of course to a higher speed of weight gain of ablated mice when compared to mice where the SNS is functional (Figure 3.7 D). When compared to C57BL/6 mice, the difference in weight gain is

enormous (Figure 3.7 E). While sympathectomized mice gain 135 % of weight after 1 month in HFD, C57BL/6 mice only gain 20 % of weight after the same period in HFD.

Apart from HFD, a regimen of HFD followed by ND (twice) was also given to mice in order to mimic a yo-yo diet regimen (Figure 3.8 A). It was demonstrated that diet-induced obesity is irreversible in sympathectomized mice as these mice are not able to lose weight as easily as control mice when fed with ND. In addition, it was verified that in a second round of HFD followed by a ND, the capacity to lose weight is even more compromised than in a first round of the same diet regimen. It could be thought that the aforementioned differences in weight gain were not directly a consequence of sympathectomy but were in fact sympathectomy-mediated differences in food intake. Indeed this is not the case because food intake was measured (Figure 3.8 B) and there was no significant difference between ablated and non-ablated mice. Nose-to-anal distance was measured in order to evaluate the differences in mice BMI (Figure 3.8 C). The results indicate that in ND regimen little difference is noticed, but the same does not happen in HFD, where the BMI of sympathectomized mice is significantly higher than the BMI of control mice. This effect reflects once again the weight gain of ablated mice when in HFD.

It was previously reported that after application of the 6-hydroxydopamine neurotoxin, the synthesis of catecholamines is increased, but it was also shown that, after two weeks, catecholamines level returns to normal [72]. It could be the case that the differences in weight seen on this work (Figure 3.7 B) were a consequence of the presence of catecholamines induced by sympathectomy. To exclude this hypothesis, HFD was given to mice only after 2 weeks of PEGyDT injections (Figure 3.8 D). As the profile of weight gain is similar to the one previously presented (Figure 3.7 B), it is possible to conclude that the higher increase in weight is not related to catecholamines production.

After establishing the effect of different diet regimens in sympathectomized mice, it was possible to show the causality that the MONA LISA hypothesis was lacking. It is the absence of SNS that leads to an obesogenic state.

Apart from the effect of different diet regimens, also metabolic parameters were measured in order to understand more deeply the consequences of sympathectomy. Thus, metabolic parameters such as blood glucose and insulin were measured in ND and every week after mice were fed with an HFD. Only the results of ND and after 5 weeks of HFD are presented as these are the ones representing the most significant values. As expected, an overnight period of fasting is not enough to have differences in weight loss (Figure 3.9 A), nevertheless it is possible to see that, after a period of 5 weeks in HFD, mice lose less weight when food deprived for one night when compared to the same period of deprivation in ND. It was demonstrated that the ablation does not cause changes both in blood glucose (Figure 3.9 D) and insulin (Figure 3.9 E) in a fasting steady state. The only differences are the increase of blood glucose and the decrease of blood insulin after a period of HFD, but these are not different from what is expected and they are also present on controls [73,74]. However, sympathectomy does affect glucose tolerance. Sympathectomized mice present a glucose intolerance state since the very beginning (ND), while control mice only present this deficiency after 5 weeks in HFD (Figure 3.9 B and C). It was reported that sympathetic activity increases glucose uptake in adipose organs [75]. Hence, it is expected that after sympathectomy the glucose uptake is impaired and consequently, sympathectomized mice present glucose intolerance, independently of food regimen.

Weight control is intimately related with thermogenesis because chemical energy is transformed in heat by brown adipose tissue (BAT) [76,77]. Hence, sympathectomized mice were exposed to a temperature challenge (4 ^{o}C) for a period of 8 h. The weight loss once again is similar to control mice (Figure 3.10 A), but the same does not happen with body temperature (Figure 3.10 B), as sympathectomized mice are unable to maintain it. In rodents, thermogenesis mainly occurs in BAT, which responds to activation of SNS [7]. The incapacity to maintain the body temperature is then explained by the lack of activation of sympathetic activity, which in consequence does not activate thermogenesis in BAT.

After performing the loss of function of SNS, its gain of function was also studied. One way to achieve this was to use AMPH, which is a sympathomimetic drug that is thought to act exclusively on the brain to suppress food intake. It was reported that AMPH is an anorexigenic drug and the data reveals that this is true because the food intake is inhibited in mice that were submitted to AMPH injections (Figure 3.11 A). Nevertheless, some other mechanism has to be present, as mice that were pair-fed to the ones administered with AMPH had an increase in body weight similar to mice administered with vehicle (Figure 3.11 B). After ceasing AMPH injections, the results indicate that the anorexigenic effect is no more present, because differences in food intake are not significant (Figure 3.11 C) and also mice that were previously

administered with AMPH injections have a higher increase in weight when compared to the ones that were only administered with vehicle (Figure 3.11 D). This increase in weight is described as the rebound effect (emergence of the symptoms that were controlled during medication administration, after ceasing it) [78].

It could be the case that the additional effect of AMPH was somehow related to the SNS. To test this hypothesis, the body weight difference between sympathectomized mice administered with AMPH or PBS and non-sympathectomized mice administered with AMPH or PBS was analyzed (Figure 3.12 A and B). It was demonstrated that the effect of AMPH in weight is higher on animals that have an intact SNS (Figure 3.12 C), suggesting that the SNS is required for AMPH effects.

When SNS is activated using AMPH, C57BL/6 mice are protected from obesogenic effects of HFD. In addition, using the tool developed in the beginning of this work (PEGyDT-mediated sympathectomy), an additional mechanism for AMPH was shown and the results indicate that non-sympathectomized mice are more prone to be protected from obesity than sympathectomized mice when AMPH is administered.

Although it was never demonstrated, this work was developed assuming that inguinal fat depot in the body is innervated as previously believed (thus a side project was performed to clearly demonstrate adipose organ innervation) [79,80]. Many diseases, such as cardiomyopathy or breast cancer, owe its diagnostic to the visualization of anatomical structures within an organ. However, this possibility is not open for a disease like obesity as a result of the absence of clear anatomical maps of the adipose organ. Clear anatomical maps of inguinal and visceral fat organs could provide cues onto the physiology of the fat organ. Phenotypic switches of inguinal to visceral fat in mutant mice have been documented using molecular markers [81]. However, the anatomical correlate of this molecular switch is unknown. This is particularly important, given the dual role of inguinal and visceral fat in the onset of morbid obesity.

To overcome, at least in part, this lack of knowledge, OPT technique coupled to tissue clearing was used to reveal in detail the anatomy of two adipose organs: the inguinal and the epididymal fat (Figure 3.13 and Figure 3.14). OPT coupled to tissue clearing offers new methodological platform for fat organ phenotyping and has the advantage of being a cost effective system to implement. OPT is suitable for imaging samples that are much larger than those imaged with confocal or multiphoton microscopy, and has higher spatial resolution than CT scans. Thin cross-sectional CT radiographs have been used to measure total body fat content and this is the only technique that allows quantification of intra-abdominal fat [34–36]. Whole body MRI was used to quantify and study different body fat depots and it gives a fast, reliable and unbiased measurement of the volume of adipose tissue [34]. However, the spatial magnitude of these techniques is not compatible with the resolution requirements for samples with sizes in the order of 1 to 1.5 cm.

It was presented an alternative technique that, without immunohistochemical labelling, enables to visualize intact structures within large size cleared organs. This is reasonable because of OPT ability to work not only with fluorescent, but also with non-fluorescent contrasts.

In this work, anatomical differences between inguinal and epididymal adipose organs were shown. The inguinal and the epididymal fat show a different type of organization that was never been described in the literature. Richly vascularized and innervated inguinal fat encloses the lymph node and is compartmentalized in lobe-like structures (Figure 3.16 and Figure 3.17). On the other hand, the distribution of the epididymal fat is rather homogeneous (Figure 3.19). The inguinal and visceral fat pads are of a different embryonic origin and their divergent anatomy and function remain to be studied. OPT results support the idea that these two fat depots might have different functions, as a consequence of its anatomical differences.

To conclude, inguinal and visceral fat pads were imaged, whole organ reconstruction was performed and 3D organization was described in detail. It was possible to detect mutually exclusive anatomical features that are unique in each pad. It was detect the presence of lymph nodes and lobe-like structures in inguinal fat, but not in visceral fat. Reciprocally, visceral fat has granule-like structures that do not exist in inguinal fat (Figure 3.20), but the biological significance of these anatomical features has yet to be unraveled.

5. Conclusion and Future perspectives

DT was modified using two strategies: PEGylation and maleimidation in order to ablate the SNS without damaging the CNS. Maleimidation proved not to be a good strategy because it led to DT loss of functionality, but the same did not happen with PEGylation. Thus, PEGyDT-mediated sympathectomy was developed to specifically ablate the SNS, so the main aim of this work was achieved.

Causality in the MONA LISA hypothesis was demonstrated performing functional studies in sympathectomized mice. The role of SNS in obesity was also unraveled by these studies, achieving another aim of this work. It was demonstrated that it has an obesogenic irreversible effect and also that it impairs not only glucose tolerance but also thermogenesis.

While studying the effects of AMPH in sympathectomized mice, an additional mechanism of action for this anti-obesity drug was described, which shows that a functional SNS is required for AMPH action.

Finally, a further study (beyond the aims of this work) was performed, in which the neuroanatomy of inguinal and epididymal adipose organs was revealed by OPT. It was demonstrated that inguinal fat contains a lymph node and is compartmentalized in lobes, but these structures are not present in the epididymal adipose organ, in which granular substructures were observed.

To complement this work and answer questions that were raised by the results obtained, some additional studies could be performed, such as:

- Determine if PEGyDT is in fact not crossing the BBB, using endothelial cells to mimic the BBB;

- Study the influence of sympathectomy in heart, as it is known that it is an extremely innervated organ [82];

- Modify AMPH in such a way that it does not reach the brain, but remains active to exert its activity in SNS;

- Understand more deeply the anatomical differences between inguinal and epididymal adipose organs and its influence on biological function.

6. References

1. Rodgers, R. J., Tschop, M. H. & Wilding, J. P. H. Anti-obesity drugs: past, present and future. *Dis. Model. Mech.* **5,** 621–626 (2012).

2. Kim, G. W., Lin, J. E., Blomain, E. S. & Waldman, S. A. Antiobesity Pharmacotherapy: New Drugs and Emerging Targets. *Clin. Pharmacol. Ther.* **95,** 53–66 (2013).

3. WHO. Noncommunicable diseases - Obesity. *http://www.euro.who.int/en/health-topics/noncommunicable-diseases/obesity* (2015).

4. WHO. Nutrition topics - Controlling the global obesity epidemic. *http://www.who.int/nutrition/topics/obesity/en/* (2015).

5. WHO. Global Health Observatory (GHO) data - Obesity: Situation and trends. *http://www.who.int/gho/ncd/risk_factors/obesity_text/en/* (2015).

6. Ricca, V., Castellini, G., Mannucci, E., Monami, M., Ravaldi, C., Gorini Amedei, S., Sauro, C. L., Rotella, C. M. & Faravelli, C. Amphetamine derivatives and obesity. *Appetite* **52,** 405–409 (2009).

7. Wilding, J. Obesity treatment. *BMJ* **315,** 997–1001 (1997).

8. Goldstein, J. & Potvin, H. Long-term weight loss: the effect of pharmacologic agent. *Am. J. Clin. Nutr.* **60,** 647–657 (1994).

9. WHO. Media centre - Obesity and overweight: Fact sheet Nº 311. *http://www.who.int/mediacentre/factsheets/fs311/en/* (2015).

10. Carter, R., Mouralidarane, A., Ray, S., Soeda, J. & Oben, J. Recent advancements in drug treatment of obesity. *Clin. Med. (Northfield. Il).* **12,** 456–460 (2012).

11. National Institute of Diabetes and Digestive and Kidney Diseases. Prescription Medications for the Treatment of Obesity. *NIH Publications*. **7,** 1-8 (2007)

12. Mancini, M. C. & Halpern, A. Pharmacological treatment of obesity. *Arq. Bras. Endocrinol. Metabol.* **50,** 377–389 (2006).

13. Kushner, R. F., Apovian, C. M. & Fujioka, K. Obesity consults-comprehensive obesity management in 2013: Understanding the shifting paradigm. *Obesity* **21,** S3-S13 (2013).

14. Dixon, J. B. Weight loss medications: Where do they fit in? *Aust. Fam. Physician* **35,** 576–579 (2006).

15. García, L. C., Ramos-Leví, A., Lopera, C. M. & Herrera, M. A. R. Update on pharmacology of obesity: benefits and risks. *Nutr. Hosp.* **28 Suppl 5,** 121–127 (2013).

16. Yanovski, S. Z. & Yanovski, J. A. Long-term drug treatment for obesity: a systematic and clinical review. *JAMA* **311,** 74–86 (2014).

17. Bray, G. A. Medical treatment of obesity: The past, the present and the future. *Best Pract. Res. Clin. Gastroenterol.* **28,** 665–684 (2014).

18. Joo, J. K. & Lee, K. S. Pharmacotherapy for Obesity. *J. Menopausal Med.* **20,** 90–96 (2014).

19. Bray, G. A. A concise review on the therapeutics of obesity. *Nutrition* **16,** 953–960 (2000).

20. Hiatt, W. R., Thomas, A. & Goldfine, A. B. What cost weight loss? *Circulation* **125,** 1171–1177 (2012).

21. Heal, D. J., Smith, S. L., Gosden, J. & Nutt, D. J. Amphetamine, past and present - a pharmacological and clinical perspective. *J. Psychopharmacol.* **27,** 479–496 (2013).

22. Nelson, D. L. & Gehlert, D. R. Central nervous system biogenic amine targets for control of appetite and energy expenditure. *Endocrine* **29,** 49–60 (2006).

23. Inchiosa, M. A. Experience (mostly negative) with the use of sympathomimetic agents for weight loss. *J. Obes.* **2011,** doi: 10.1155/2011/764584 (2011).

24. Rucker, D., Padwal, R., Li, S. K., Curioni, C. & Lau, D. C. W. Long term pharmacotherapy for obesity and overweight: updated meta-analysis. *BMJ* **335,** 1194–1199 (2007).

25. Padwal, R. S., Rucker, D., Li, S. K., Curioni, C. & Lau, D. C. W. Long-term pharmacotherapy for obesity and overweight. *The Cochrane* **1**, 1–96 (2009).

26. Halaas, J. L., Gajiwala, K. S., Maffei, M., Cohen, S. L., Chait, B. T., Rabinowitz, D., Lallone, R. L., Burley, S. K. & Friedman, J. M. Weight-reducing effects of the plasma protein encoded by the obese gene. *Science* **269,** 543–546 (1995).

27. Domingos, A. I., Vaynshteyn, J., Voss, H. U., Ren, X., Gradinaru, V., Zang, F., Deisseroth, K., de Araujo, I. E. & Friedman, J. Leptin regulates the reward value of nutrient. *Nat. Neurosci.* **14,** 1562–1568 (2011).

28. Barzilai, N., She, L., Liu, B. Q., Vuguin, P., Cohen, P., Wang, J. & Rossetti, L. Surgical removal of visceral fat reverses hepatic insulin resistance. *Diabetes* **48,** 94–98 (1999).

29. Chau, Y., Bandiera, R., Serrels, A., Martínez-Estrada, O. M., Qing, W., Lee, M., Slight, J., Thornburn, A., Berry, R., McHaffie, S., Stimson, R. H., Walker, B. R., Chapuli, R. M., Schedl, A. & Hastie, N. Visceral and subcutaneous fat have different origins and evidence supports a mesothelial source. *Nat. Cell Biol.* **16,** 367–375 (2014).

30. Cinti, S. Transdifferentiation properties of adipocytes in the adipose organ. *Am. J. Physiol. - Endocrinol. Metab.* **297,** E977–E986 (2009).

31. Cinti, P. S. Anatomy of the adipose organ. *Eat. Weight Disord. - Stud. Anorexia, Bulim. Obes.* **5,** 132–142 (2014).

32. Conchello, J. A. & Lichtman, J. W. Optical sectioning microscopy. *Nat. Methods* **2,** 920–931 (2005).

33. Helmchen, F. & Denk, W. Deep tissue two-photon microscopy. *Nat. Methods* **2,** 932–940 (2005).

34. Thomas, E. L., Saeed, N., Hajnal, J. V., Brynes, A., Goldstone, A. P., Frost, G. & Bell, J. D. Magnetic resonance imaging of total body fat. *J. Appl. Physiol.* **85,** 1778–1785 (1998).

35. Hu, H. H., Perkins, T. G., Chia, J. M. & Gilsanz, V. Characterization of Human Brown Adipose Tissue by Chemical-Shift Water-Fat MRI. *AJR. Am. J. Roentgenol.* **200,** 177–183 (2013).

36. Borkan, G. A., Gerzof, S. G., Robbins, A. H., Hults, D. E., Silbert, C. K. & Silbert, J. E. Assessment of abdominal fat content by computed tomography. *Am. J. Clin. Nutr.* **36,** 172–177 (1982).

37. Sharpe, J. Optical Projection Tomography. *Annu. Rev. Biomed. Eng.* **6,** 209–228 (2004).

38. Quintana, L. & Sharpe, J. Optical Projection Tomography of Vertebrate Embryo Development. *Cold Spring Harb. Protoc.* **2011,** 586-594 (2011).

39. Bray, G. A. Obesity, a disorder of nutrient partitioning: the MONA LISA hypothesis. *J. Nutr.* **121,** 1146–1162 (1991).

40. Messina, G., De Luca, V., Viggiano, A., Ascione, A., Iannaccone, T., Chieffi, S. & Monda, M. Autonomic nervous system in the control of energy balance and body weight: Personal contributions. *Neurol. Res. Int.* **2013,** doi: 10.1155/2013/639280 (2013).

41. Da Vinci, Leonardo. *Mona Lisa*. 1503-1506. Oil on wood. Louvre, Paris.

42. Young, J. B. & Landsberg, L. Suppression of sympathetic nervous system during fasting. *Obes. Res.* **5,** 646–649 (1997).

43. Young, J. B. & Landsberg, L. Stimulation of sympathetic nervous system during sucrose feeding. *Nature* **269,** 615–617 (1977).

44. Houle, M. S. & Billman, G. E. Low-frequency component of the heart rate variability spectrum: a poor marker of sympathetic activity. *Am. J. Physiol.* **276,** H215–H223 (1999).

45. Kos, C. H. Cre/loxP system for generating tissue-specific knockout mouse models. *Nutr. Rev.* **62,** 243–246 (2004).

46. Feil, S., Valtcheva, N. & Feil, R. (2009) Inducible Cre Mice In Human Press - Springer Protocols (Second Edition), *Gene Knockout Protocols* (pp. 343-364). New York, NY.

47. Inlay, M. A., Choe, V., Bharathi, S., Fernhoff, N. B., Baker, J. R., Weissman, I. L. & Choi, S. K. Synthesis of a photocaged tamoxifen for light-dependent activation of Cre-ER recombinase-driven gene modification. *Chem. Commun. (Camb).* **49,** 4971–4973 (2013).

48. Buch, T., Heppner, F. L., Tertilt, C., Heinen, T. J. a J., Kremer, M., Wunderlich, F. T., Jung, S. & Waisman, A. A Cre-inducible diphtheria toxin receptor mediates cell lineage ablation after toxin administration. *Nat. Methods* **2,** 419–426 (2005).

49. Collier, R. J. Diphtheria toxin: mode of action and structure. *Bacteriol. Rev.* **39,** 54–85 (1975).

50. Chenal, A., Nizard, P. & Gillet, D. Structure and Function of Diphtheria Toxin: From Pathology To Engineering. *Toxin Rev.* **21,** 321–359 (2002).

51. Ratts, R. & Murphy, J. R. Diphtheria toxin, diphtheria-related fusion protein toxins, and the molecular mechanism of their action against eukaryotic cells. *Microb. Protein Toxins Top. Curr. Genet.* **11,** 1–20 (2005).

52. Uchida, T. Diphtheria toxin. *Pharmacol. Ther.* **19,** 107–122 (1982).

53. Rolf, J. M., Gaudin, H. M., Tirrell, S. M., MacDonald, A. B. & Eidels, L. Anti-idiotypic antibodies that protect cells against the action of diphtheria toxin. *Proc. Natl. Acad. Sci. U. S. A.* **86,** 2036–2039 (1989).

54. Roberts, M. J., Bentley, M. D. & Harris, J. M. Chemistry for peptide and protein PEGylation. *Adv. Drug Deliv. Rev.* **64,** 116–127 (2012).

55. Harris, J. M., Martin, N. E. & Modi, M. Pegylation: a novel process for modifying pharmacokinetics. *Clin. Pharmacokinet.* **40,** 539–551 (2001).

56. Harris, J. M. & Chess, R. B. Effect of pegylation on pharmaceuticals. *Nat. Rev. Drug Discov.* **2,** 214–221 (2003).

57. Boutureira, O. & Bernardes, G. J. L. Advances in Chemical Protein Modification. *Chem. Rev.* **115,** 2174-2195 (2015).

58. Veronese, F. M. & Pasut, G. PEGylation, successful approach to drug delivery. *Drug Discov. Today* **10,** 1451–1458 (2005).

59. Jevševar, S., Kunstelj, M. & Porekar, V. G. PEGylation of therapeutic proteins. *Biotechnol. J.* **5,** 113–128 (2010).

60. Milla, P., Dosio, F. & Cattel, L. PEGylation of Proteins and Liposomes: a Powerful and Flexible Strategy to Improve the Drug Delivery. *Curr. Drug Metab.* **13,** 105–119 (2012).

61. Payne, R. W., Murphy, B. M. & Manning, M. C. Product development issues for PEGylated proteins. *Pharm. Dev. Technol.* **16,** 423–440 (2011).

62. Ottow, K. E., Lund-Olesen, T., Maury, T. L., Hansen, M. F. & Hobley, T. J. A magnetic adsorbent-based process for semi-continuous PEGylation of proteins. *Biotechnol. J.* **6,** 396–409 (2011).

63. González, M. & Vaillard, S. E. Evolution of Reactive mPEG Polymers for the Conjugation of Peptides and Proteins. *Curr. Org. Chem.* **17,** 1-24 (2013).

64. Veronese, F. M. Peptide and protein PEGylation: a review of problems and solutions. *Biomaterials* **22,** 405–417 (2001).

65. Veronese, F. M. & Harris, J. M. Introduction and overview of peptide and protein pegylation. *Adv. Drug Deliv. Rev.* **54,** 453–456 (2002).

66. Zalipsky, S. & Harris, J. M. (1997) Introduction to chemistry and biological applications of poly (ethylene glycol) In Harris, J. M. & Zalipsky, S. (Volume 680), *Poly(ethylene glycol) - Chemistry and Biological Applications* (pp. 1-13). Washington, D.C.

67. Hershfield, M. S. (1997) Biochemistry and Immunology of Poly (ethylene glycol)-Modified Adenosine Deaminase (PEG-ADA). In Harris, J. M. & Zalipsky, S. (Volume 680), *Poly(ethylene glycol) - Chemistry and Biological Applications* (pp. 145-154). Washington, D.C.

68. Mantovani, G., Lecolley, F., Tao, L., Haddleton, D. M., Clerx, J., Cornelissen, J. J. L. M. & Velonia, K. Design and synthesis of N-maleimido-functionalized hydrophilic polymers via copper-mediated living radical polymerization: A suitable alternative to pegylation chemistry. *J. Am. Chem. Soc.* **127,** 2966–2973 (2005).

69. Smith, M. E. B., Caspersen, M. B., Robinson, E., Morais, M., Maruani, A., Nunes, J. P. M., Nicholls, K., Saxton, M. J., Caddick, S., Baker, J. R. & Chudasama, V. A platform for efficient, thiol-stable conjugation to albumin's native single accessible cysteine. *Org. Biomol. Chem.* **13,** 7946–7949 (2015).

70. Schindelin, J., Arganda-Carreras, I., Frise, E., Kaynig, V., Longair, M., Pietzsch, T., Preibisch, S., Rueden, C., Saalfeld, S., Schmid, B., Tinevez, J. Y., White, D. J., Hartenstein, V., Eliceiri, K., Tomancak, P. & Cardona, A. Fiji: an open-source platform for biological-image analysis. *Nat. Methods* **9,** 676–682 (2012).

71. Zeng, W., Pirzgalska, R. M., Pereira, M. M. A., Kubasova, N., Barateiro, A., Seixas, E., Lu, Y. H., Kozlova, A., Voss, H., Martins, G. G., Friedman, J. M. & Domingos, A. I. Sympathetic Neuro-adipose Connections Mediate Leptin-Driven Lipolysis. *Cell* **163**, 84-94 (2015).

72. Stachowiak, M. K., Fluharty, S. J., Stricker, E. M., Zigmond, M. J. & Kaplan, B. B. Molecular adaptations in catecholamine biosynthesis induced by cold stress and sympathectomy. *J. Neurosci. Res.* **16,** 13–24 (1986).

73. Surwit, R. S., Kuhn, C. M., Cochrane, C., McCubbin, J. A. & Feinglos, M. N. Diet-induced type II diabetes in C57BL/6J mice. *Diabetes* **37,** 1163–1167 (1988).

74. Winzell, M. S. & Ahrén, B. The high-fat diet-fed mouse: a model for studying mechanisms and treatment of impaired glucose tolerance and type 2 diabetes. *Diabetes* **53 Suppl 3,** S215–S219 (2004).

75. Nonogaki, K. New insights into sympathetic regulation of glucose and fat metabolism. *Diabetologia* **43,** 533–549 (2000).

76. Lowell, B. B. & Spiegelman, B. M. Towards a molecular understanding of adaptive thermogenesis. *Nature* **404,** 652–660 (2000).

77. Wu, J., Cohen, P. & Spiegelman, B. M. Adaptive thermogenesis in adipocytes: Is beige the new brown? *Genes Dev.* **27,** 234–250 (2013).

78. Cox, D. J., Moore, M., Burket, R., Merkel, R. L., Mikami, A. Y. & Kovatchev, B. Rebound effects with long-acting amphetamine or methylphenidate stimulant medication preparations among adolescent male drivers with attention-deficit/hyperactivity disorder. *J. Child Adolesc. Psychopharmacol.* **18,** 1–10 (2008).

79. Bartness, T. & Bamshad, M. Innervation of mammalian white adipose tissue: implications for the regulation of total body fat. *Am. J. Physiol.* **275,** 1399–1411 (1998).

80. Bartness, T. J., Shrestha, Y. B., Vaughan, C. H., Schwartz, G. J. & Song, C. K. Sensory and sympathetic nervous system control of white adipose tissue lipolysis. *Mol. Cell. Endocrinol.* **318,** 34–43 (2010).

81. Cohen, P., Levy, J. D., Zhang, Y., Frontini, A., Kolodin, D. P., Svensson, K. J., Lo, J. C., Zeng, X., Ye, L., Khandekar, M. J., Wu, J., Gunawardana, S. C., Banks, A. S., Camporez, J. P. G., Jurczak, M. J., Kajimura, S., Piston, D. W., Mathis, D., Cinti, S., Shulman, G. I., Seale, P. & Spiegelman, B. M. Ablation of PRDM16 and beige adipose causes metabolic dysfunction and a subcutaneous to visceral fat switch. *Cell* **156,** 304–316 (2014).

82. Shanks, J. & Herring, N. Peripheral cardiac sympathetic hyperactivity in cardiovascular disease: role of neuropeptides. *Am. J. Physiol. Regul. Integr. Comp. Physiol.* **305,** 1411–1420 (2013).

7. Appendix

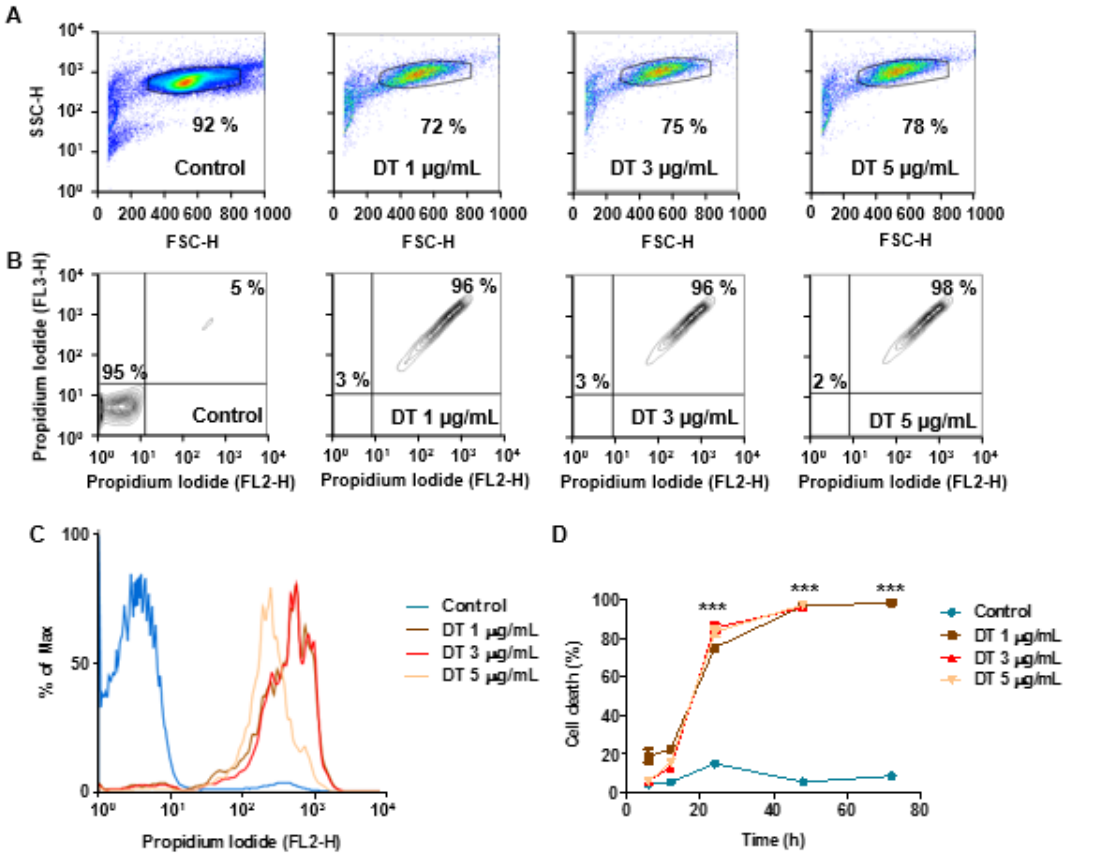

Figure 7.1 – DT concentration test on HeLa cells. A) Gating strategy of FACS data obtained using HeLa cells for control and DT 1 µg/mL, 3 µg/mL and 5 µg/mL after 48 h of incubation; B) Representative contour plots of control and DT 1 µg/mL, 3 µg/mL and 5 µg/mL populations after 48 h of incubation in HeLa cells; C) Representation of live and dead cell populations after 48 h of incubation with DT 1 µg/mL, 3 µg/mL and 5 µg/mL; D) Quantification of HeLa cell death during time after incubation with control and DT 1 µg/mL, 3 µg/mL and 5 µg/mL (*** $p < 0.0001$, $n = 3$). Data are represented as mean ± SEM.

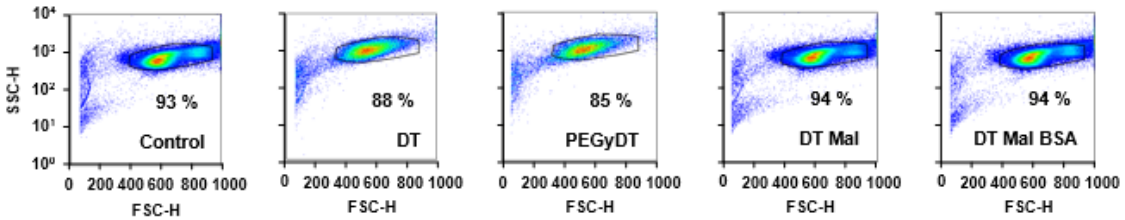

Figure 7.2 – DT functionality after modification tested on *in vitro* HeLa cell line culture. Gating strategy of FACS data obtained using HeLa cells for Control, DT, PEGyDT, DT Mal and DT Mal BSA after 48 h of incubation.

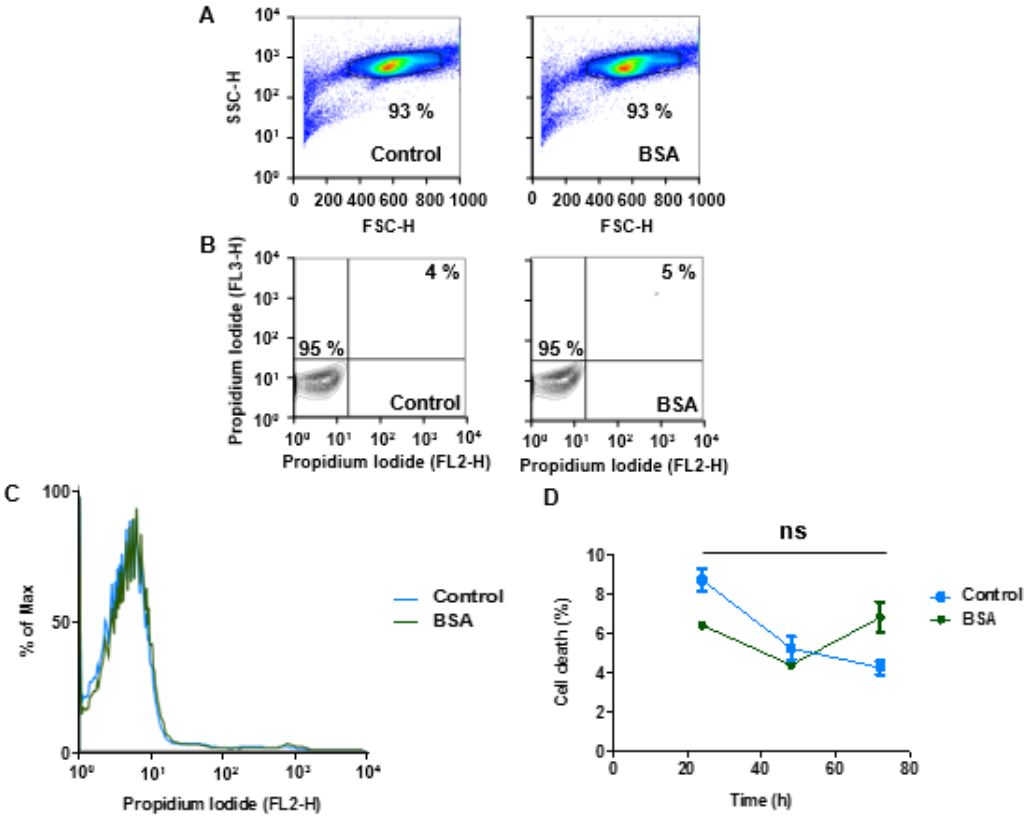

Figure 7.3 – HeLa cell line culture incubated with BSA. A) Gating strategy of FACS data obtained using HeLa cells for Control and BSA 2.25 mg/mL; B) Representative contour plots of Control and BSA 2.25 mg/mL populations after 48 h of incubation in HeLa cells; C) Representation of live and dead cell populations after 48 h of incubation with BSA 2.25 mg/mL in HeLa cells; D) Quantification of HeLa cell death during time after incubation with BSA 2.25 mg/mL (n = 3). Data are represented as mean ± SEM.

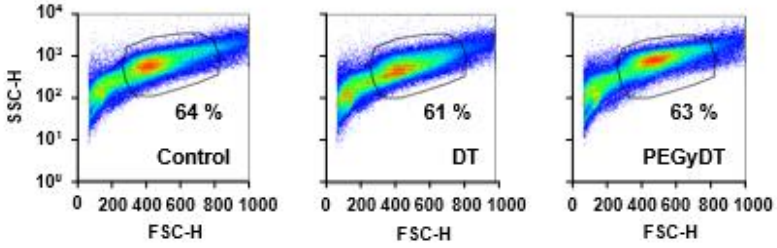

Figure 7.4 – DT functionality after modification tested *in vitro* on primary cell culture of macrophages derived from the BM of Rosa26Cre-ER(T2); LSL-DTR mice after tamoxifen was administered *in vivo*. Gating strategy of FACS data obtained using HeLa cells for DT and PEGyDT after 48 h of incubation.

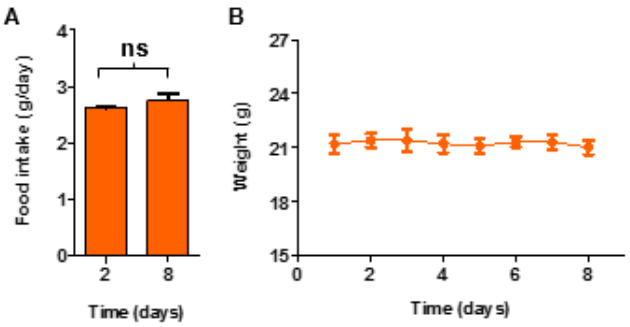

Figure 7.5 – PBS administration does not affect food intake and body weight. A) Food intake on the first and last day of administration of PBS (n = 6); B) Mice weight during daily administration of PBS (n = 6). Data are represented as mean ± SEM.

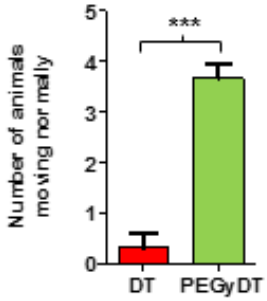

Figure 7.6 – DT, but not PEGyDT, administration affects normal movement of mice (* p < 0.0001, n = 3).** Data are represented as mean ± SEM.

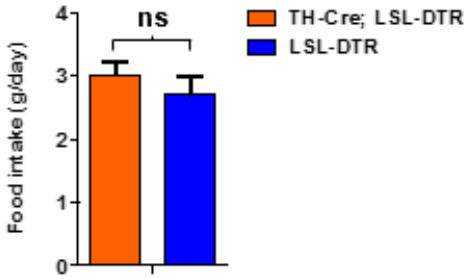

Figure 7.7 – Food intake during HFD feeding 2 weeks after SNS ablation (n = 5-6). Data are represented as mean ± SEM.

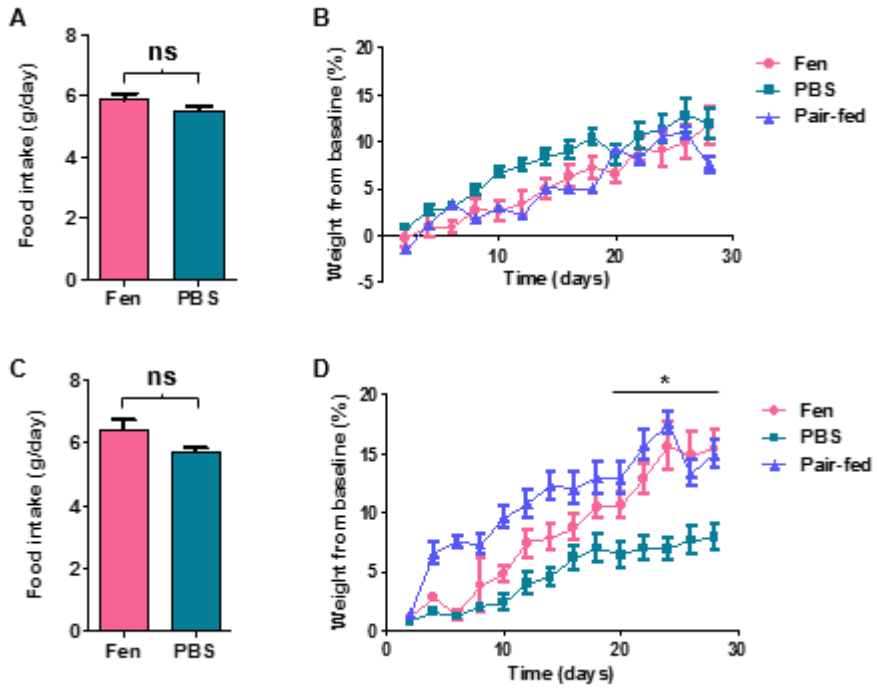

Figure 7.8 – Differences in weight and in food intake on a HFD regimen. A) Food intake during the period of Fen administration (n = 4-5); B) Weight gain during the period of Fen administration (n = 4-5); C) Food intake after ceasing Fen administration (n = 4-5); D) Weight gain after ceasing Fen administration (* p < 0.01, n = 4-5). Data are represented as mean ± SEM.

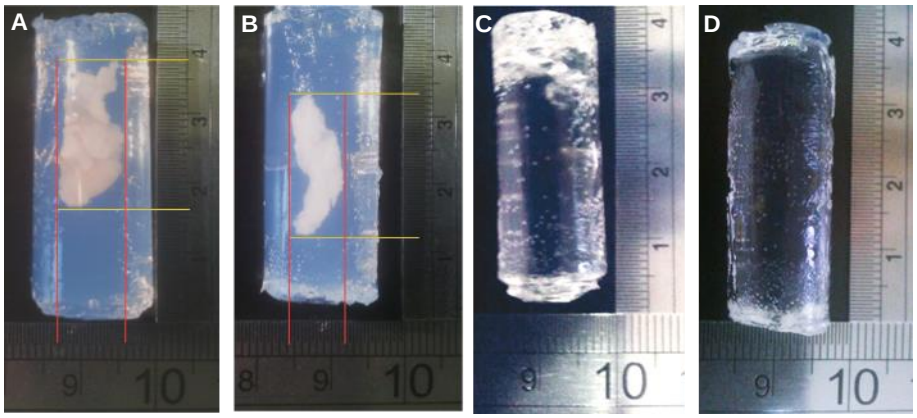

Figure 7.9 – Adipose organs in agarose, low gelling temperature before and after clearing procedure. A) Epididymal adipose organ before clearing; B) Inguinal adipose organ before clearing; C) Epididymal adipose organ after clearing; D) Inguinal adipose organ after clearing.